Aerosol analysis and forecast in the European Centre for Medium-Range Weather Forecasts Integrated Forecast System: 3. Evaluation by means of case studies

A. Mangold,[1] H. De Backer,[1] B. De Paepe,[1] S. Dewitte,[1] I. Chiapello,[2] Y. Derimian,[2] M. Kacenelenbogen,[2,3] J.-F. Léon,[2] N. Huneeus,[4] M. Schulz,[4] D. Ceburnis,[5] C. O'Dowd,[5] H. Flentje,[6] S. Kinne,[7] A. Benedetti,[8] J.-J. Morcrette,[8] and O. Boucher[9]

Received 5 August 2010; revised 19 November 2010; accepted 2 December 2010; published 8 February 2011.

[1] A near real-time system for assimilation and forecasts of aerosols, greenhouse and trace gases, extending the ECMWF Integrated Forecasting System (IFS), has been developed in the framework of the Global and regional Earth-system Monitoring using Satellite and in-situ data (GEMS) project. The GEMS aerosol modeling system is novel as it is the first aerosol model fully coupled to a numerical weather prediction model with data assimilation. A reanalysis of the period 2003–2009 has been carried out with the same system. During its development phase, the aerosol system was first run for the time period January 2003 to December 2004 and included sea salt, desert dust, organic matter, black carbon, and sulfate aerosols. In the analysis, Moderate Resolution Imaging Spectroradiometer (MODIS) total aerosol optical depth (AOD) at 550 nm over ocean and land (except over bright surfaces) was assimilated. This work evaluates the performance of the aerosol system by means of case studies. The case studies include (1) the summer heat wave in Europe in August 2003, characterized by forest fire aerosol and conditions of high temperatures and stagnation, favoring photochemistry and secondary aerosol formation, (2) a large Saharan dust event in March 2004, and (3) periods of high and low sea salt aerosol production. During the heat wave period in 2003, the linear correlation coefficients between modeled and observed AOD (550 nm) and between modeled and observed PM2.5 mass concentrations are 0.82 and 0.71, respectively, for all investigated sites together. The AOD is slightly and the PM2.5 mass concentration is clearly overestimated by the aerosol model during this period. The simulated sulfate mass concentration is significantly correlated with observations but is distinctly overestimated. The horizontal and vertical locations of the main features of the aerosol distribution during the Saharan dust outbreak are generally well captured, as well as the timing of the AOD peaks. The aerosol model simulates winter sea salt AOD reasonably well, however, showing a general overestimation. Summer sea salt events show a better agreement. Overall, the assimilation of MODIS AOD data improves the subsequent aerosol predictions when compared with observations, in particular concerning the correlation and AOD peak values. The assimilation is less effective in correcting a positive (PM2.5, sulfate mass concentration, Angström exponent) or negative (desert dust plume AOD) model bias.

Citation: Mangold, A., et al. (2011), Aerosol analysis and forecast in the European Centre for Medium-Range Weather Forecasts Integrated Forecast System: 3. Evaluation by means of case studies, *J. Geophys. Res.*, *116*, D03302, doi:10.1029/2010JD014864.

[1]Observations Department, Royal Meteorological Institute of Belgium, Brussels, Belgium.
[2]Laboratoire d'Optique Atmosphérique, CNRS/Université de Lille 1, Villeneuve d'Ascq, France.
[3]Now at ORAU/NASA Ames Research Center, Moffett Field, California, USA.
[4]Laboratoire des Sciences du Climat et de l'Environnement, CEA/CNRS/UVSQ, Gif-sur-Yvette, France.
[5]School of Physics and Centre for Climate and Air Pollution Studies, Environmental Change Institute, National University of Ireland Galway, Galway, Ireland.
[6]Meteorologisches Observatorium Hohenpeissenberg, Deutscher Wetterdienst, Hohenpeissenberg, Germany.
[7]Max-Planck Institute for Meteorology, Hamburg, Germany.
[8]European Centre for Medium-range Weather Forecasts, Reading, UK.
[9]Met Office Hadley Centre, Exeter, UK.

0148-0227/11/2010JD014864

1. Introduction

[2] Within the European Commission's Framework Programme 6 project Global and regional Earth-system Monitoring using Satellite and in-situ data (GEMS) [*Hollingsworth et al.*, 2008], near real-time assimilation and forecasts of aerosols, greenhouse gases and reactive gases have been developed, either by integration in or coupling to the ECMWF (European Centre for Medium-Range Weather Forecast) Integrated Forecast System (IFS) code. A reanalysis of the period 2003–2009 has been carried out with the same system. During its development phase, the aerosol system was first run for the time period January 2003 to December 2004 and included sea salt, desert dust, organic matter, black carbon and sulfate aerosols.

[3] The interest for regional to global aerosol modeling stems essentially from a climate change and an air quality perspective. The main driver for global-scale modeling of aerosols is the interest in the aerosol direct and indirect effects on climate, which are responsible for a large uncertainty in radiative forcing and future climate change [*Intergovernmental Panel on Climate Change* (*IPCC*), 2007]. The impacts of aerosols on air quality and health are well recognized and a number of air quality models are capable of simulating particulate matter [e.g., *Vautard et al.*, 2007].

[4] There is a wealth of measurements on aerosols but integration of these measurements is mostly missing. *Barrie et al.* [2004] reviewed the multiple data sets on atmospheric aerosols from surface, airborne and satellite-borne measurements, and indicated data assimilation as an important tool to integrate these observations. However, aerosol modeling is mainly done within climate and air quality models. There have been a few attempts to assimilate aerosol satellite products [e.g., *Collins et al.*, 2001; *Yu et al.*, 2004] or radiances [*Weaver et al.*, 2007] into global climate or chemical transport models, but rather with the aim to understand the aerosol atmospheric cycle than to monitor it. Recently, *Zhang et al.* [2008] presented an aerosol data assimilation package within the U.S. Naval Research Laboratory's Aerosol Analysis and Prediction System for aerosol forecasting purposes. A two-dimensional variational technique was applied to assimilate MODIS (Moderate Resolution Imaging Spectroradiometer) level-3 over-water total aerosol optical depth (AOD) at 550 nm.

[5] The GEMS project therefore represents an unprecedented effort to model atmospheric aerosols in the context of operational numerical weather prediction (NWP) taking an advantage of state-of-the-art meteorological information and data assimilation techniques. The GEMS aerosol analysis and forecast modules provide a preoperational monitoring and forecasting tool on the global scale, which can be useful for accurate monitoring of natural and anthropogenic aerosol four-dimensional distribution for climate studies, improvement of the overall meteorology within NWP, boundary conditions for regional air quality models, understanding aerosol-meteorology interactions, aerosol impacts on ecosystems (acid rain, fertilization, diffuse radiation), and improving visibility and ultraviolet radiation products.

[6] This study complements three companion papers, which detail the aerosol forward model itself [*Morcrette et al.*, 2009], the data assimilation [*Benedetti et al.*, 2009], and the overall evaluation statistics (M. Schulz et al., Aerosol analysis and forecast in the ECMWF Integrated Forecast System: 4. Model evaluation, manuscript in preparation, 2010, hereafter SchulzetalPartIV2010). SchulzetalPartIV2010 discusses the overall performance of both aerosol modeling without and with assimilation, on both global and regional scales, as well as seasonality and aerosol composition. Here, we evaluate the performance of the aerosol model before and after assimilation by means of case studies, allowing to analyze in detail the ability of the model to reproduce observed aerosol properties, concentration, transport, and their evolution on scales down to local values averaged over 3 h. Case studies offer the advantage of strong signal events with sufficient observational data available in order to judge the performance of the aerosol model to correctly predict strong aerosol signal changes, including peaks and lows. The spatial and temporal agreement with observations allows conclusions on the validity of source functions and emission data used and which parts of the aerosol model system could be improved.

[7] Case studies examined were: (1) the summer heat wave in Europe in August 2003, characterized by forest fire aerosol and conditions of high temperatures and stagnation, favoring photochemistry and secondary aerosol formation, (2) a large Saharan dust event in the beginning of March 2004, transporting the dust over the Atlantic, to Europe and South America, and (3) periods of high and low sea salt aerosol production. These cases have been selected to represent the different aerosol types, and because their proper representation by the model is relevant for the boundary conditions to be fed into European regional air quality models. Distinct events when organic matter, black carbon or sulfate were dominating were not possible to investigate because of the limits of observational data availability.

[8] Two simulations with the aerosol model were considered: the free running forward model with no assimilation of any aerosol related data (hereafter named DIRECT) [*Morcrette et al.*, 2009], and the analysis version with assimilation of MODIS total AOD data at 550 nm over ocean and land (hereafter named ASSIM) [*Benedetti et al.*, 2009].

[9] Specifically, the forecast of total and partial (for the modeled individual aerosol species) AOD and surface mass concentrations are compared to observational data, comprising AOD data from ground-based measurements and from satellite observations, surface PM2.5 measurements as well as chemically resolved EMEP data.

2. Aerosol Model

2.1. Forward Model Without Assimilation (DIRECT)

[10] The aerosol forward model [*Morcrette et al.*, 2009] contains five aerosol types: sea salt (SS), desert dust (DD), organic matter (OM), black carbon (BC), and a sulfate-related variable (SU). Total column aerosol optical depth (AOD) is calculated at 469, 550, 670, 865, 1240, 1640, and 2130 nm. Partial AODs for SS, DD, OM, BC, and SU are calculated at 550 nm. In addition, for each of the five aerosol types, the mass mixing ratio of each size bin on each of the 60 height levels is available. The forecast is restarted every 12 h from operational ECMWF analyses, with aerosol fields initialized from null concentrations on 01 December 2002, 0000 UT. The aerosols at the end of a given 12 h forecast are passed as initial conditions to the next 12 h forecast.

Forecast values are archived for 3, 6, 9, and 12 h lead time. Model resolution is $T_L159L60$ (1.125° × 1.125° grid, 60 height levels).

[11] The aerosol model includes 3 bins of SS (radius boundaries of 0.03–0.5–5–20 μm) and DD (radius boundaries of 0.03–0.55–0.9–20 μm). These limits are chosen so that roughly 10, 20, and 70% of the mass of each aerosol type lie in the three respective bins. The radii given are for dry particles. The ambient humidity is taken into account for the processes of sedimentation, wet deposition and radiation. Sources of SS and DD are interactive and calculated with surface and near-surface variables of the model [*Morcrette et al.*, 2008]. The surface flux of SS aerosol is parameterized from the 10 m wind at the free ocean surface from a hybrid scheme developed by *Schulz et al.* [2004], based on work by *Monahan et al.* [1982] for large particles and modified after *Smith and Harrison* [1998]. The source function for the emission of desert dust is adapted from work by *Ginoux et al.* [2001], and is based on a limited number of climatological parameters (fraction of bare soil, vegetation cover, orography), some observations (MODIS component of UV-VIS surface albedo), and model prognostic variables (soil moisture, 10 m wind speed, snow cover, surface and top layer temperature). Sources for OM, BC and SU are taken from the SPEW (Speciated Particulate Emission Wizard) and EDGAR (Emission Database for Global Atmospheric Research) annual or monthly mean climatologies [*Dentener et al.*, 2006], as well as from version 2 of the GFED (Global Fire Emission Database) 8 day mean emission data set [*van der Werf et al.*, 2006]. OM is distributed between 50% of hydrophilic and 50% of hydrophobic OM, whereas 80% of BC is kept as hydrophobic and 20% is considered as hydrophilic. Once emitted, the hydrophobic component is transformed into a hydrophilic one with a time constant of 1.16 per day. The sulfur cycle is represented by a simple conversion of SO_2 emissions to SO_4 [*Huneeus et al.*, 2009], and there is one aerosol size bin dedicated to SO_4. There is no stratospheric aerosol included, as stratospheric aerosol loadings were very small during the period under investigation.

[12] The package of ECMWF physical parameterizations dedicated to aerosol processes mainly follows the treatment in the LOA/LMDZ model [*Reddy et al.*, 2005]. It allows the aerosols to be advected, and the vertical diffusion and the mass-flux convection schemes to account explicitly for tracers such as aerosols. All aerosols undergo sedimentation, dry deposition and wet deposition (by large-scale and convective precipitation). The model prognostic aerosol is not interactive with the radiation scheme of the ECMWF IFS, i.e., that the radiation scheme still relies on the climatological aerosols derived from work by *Tegen et al.* [1997].

2.2. Aerosol Assimilation Scheme

[13] The aerosol assimilation scheme is part of the meteorological 4D-Var assimilation system employed operationally at ECMWF. The assimilation output, also known as analysis and referred to as ASSIM hereafter, represents the best statistical compromise between the background information (i.e., the output of a short, 15 h forecast of the aerosol model) and the observations. A detailed description is presented by *Benedetti et al.* [2009].

[14] The ASSIM simulation assimilates total aerosol optical depth data at 550 nm from MODIS on board of Terra and Aqua satellites (data collection 5). MODIS data are chosen for their reliability and availability in near real time. For a general description of MODIS AOD, see *Remer et al.* [2005], and for a description of the current MODIS AOD collection 5 data over land, see *Levy et al.* [2007]. AOD data both over ocean and land are assimilated. However, over highly reflective surfaces, such as deserts and snow covered areas, there is not sufficient contrast to discern the aerosol signal from the surface signal, and therefore, no MODIS AOD data exist over such areas. The original MODIS retrievals have a resolution of 10 × 10 km^2. Since the analysis was run at T_L159, which is approximately 120 × 120 km^2, MODIS AOD data of a grid of 0.5° × 0.5° are taken. For the application of the observation operator, MODIS data are taken at the original time, and at the specific observation location, and model aerosol fields are interpolated to this location. Over the 12 h window of the analysis, there are around 16,000 data points on average from MODIS on Aqua and Terra satellites.

[15] The observation operator for aerosol optical depth is based on optical properties, precomputed using Mie theory for the aerosol species included in the model, as in work by *Reddy et al.* [2005]. The aerosols are assumed to be externally mixed. The optimization of the distance between the background information and the MODIS observations is performed with respect to a single control variable, the total aerosol mixing ratio, defined as the sum of all bins of the individual aerosol species. Including all aerosol species and size bins in the analysis would increase the computational cost disproportionally. But, most importantly, the aerosol analysis would severely be underconstrained as one observation of total aerosol optical depth would be used to constrain the profiles of all aerosol species. At each iteration of the 4-D VAR minimization calculation, the increments in the total mixing ratio originating from the assimilation of MODIS AOD are redistributed into the mixing ratios of the individual species, according to their fractional distribution.

3. Observational Data for Evaluation

3.1. Satellite Data

[16] POLDER-2 (Polarization and Directionality of Earth's Reflectances) flew aboard ADEOS-2 (Advanced Earth Observation Satellite) from April to October 2003. POLDER-2 provided spectral, directional and polarized measurements of the solar radiation reflected by the Earth-atmosphere system. The observations had a spatial resolution of 6 × 7 km^2 and its field of view induced a 2400 km swath allowing a nearly global daily coverage. In order to increase the signal to noise ratio, the AOD retrieval algorithm is applied to 3 × 3 POLDER pixels, leading to a resolution of 18 × 21 km^2. Only cloud-free pixels selected according to the algorithm of *Bréon and Colzy* [1999] are processed. AOD is retrieved from measurements in the 670 and 865 nm channels that were equipped with polarization filters. The POLDER-2 product over ocean provides total AOD, while over land only fine-mode fraction AOD is available. The fine-mode fraction AOD of POLDER is modeled by single lognormal size distribution with geometric standard deviation of 0.4 and the mean radius varying

from 0.05 to 0.15 μm. In this study, fine-mode AOD at 865 nm is used, together with the fine-mode AOD at 550 nm, extrapolated from the measurements at 670 and 865 nm, using the Angström exponent. More details on the AOD retrieval from POLDER measurements are described by *Deuzé et al.* [2001]. A mean of all clear sky POLDER-2 observations during a day within a box of 1.125° × 1.125°, which is centered at the same coordinates as the model cell, is generated for the comparison with the daily mean GEMS aerosol product. In order to get a reasonable number of points for the comparison we do not limit the minimal number of POLDER observation that should fall within the model cell. In this analysis there are 11.95 ± 12.71 (mean ± standard deviation) POLDER-2 observations within a model cell.

[17] The Spinning Enhanced Visible and InfraRed Imager (SEVIRI) is flown on the geostationary Meteosat Second Generation-1 satellite located at 3.4°W above the equator. The SEVIRI aerosol product used here includes AOD at 630, 830 and 1610 nm with a spatial resolution of 9 × 9 km^2 and a time resolution of 15 min. The data is averaged to the 3-hourly GEMS aerosol model output. The AOD values are derived independently from the respective SEVIRI bands [*Ignatov and Stowe*, 2002], and a special cloud screening is applied [*De Paepe et al.*, 2008]. The SEVIRI aerosol product is available over ocean only, for the SEVIRI disk and for solar zenith angles smaller than 60°.

3.2. Ground-Based Data

[18] The AErosol RObotik NETwork (AERONET) [*Holben et al.*, 2001] of ground-based Sun photometer measurements provides a unique opportunity to evaluate the GEMS aerosol model. AERONET retrieval of total AOD and aerosol properties relies on measurements of direct sun radiances and radiance scans in the almucantar and azimuth planes. The AERONET Sun photometer data provide statistics on AOD and its spectral dependence (depending on the respective instrument and site, wavelengths comprise 340, 380, 440, 500, 675, 870, 1020 nm). The spectral dependence defines the Angström exponent and is an indicator for the overall aerosol size. In addition, the almucantar and azimuth plane measurements provide statistics on quantities like size distribution, fine-mode fraction (diameter smaller than 1 μm) and effective radius. For a description of the errors and quality assurance procedures for the AERONET Sun photometers, we refer to *Dubovik et al.* [2000, 2002].

[19] For this study, AERONET level 2.0 quality-assured data are used. The processed AERONET Sun and sky measurement statistics are based on the new version-2 products. For GEMS purposes, daily and 3-hourly averages are provided. For site comparisons, model data are extracted for grid cells that are centered at the coordinates closest to the measurement location. AOD data at Mace Head (sea salt comparisons) are obtained from the Global Atmosphere Watch Precision Filter Radiometers (GAWPFR) network [*Mulcahy et al.*, 2009; *Wehrli*, 2004]. Aerosol optical depth data are further complemented by UV-B AOD data (320 nm) derived from Brewer spectrophotometers. The Brewer UV-B AOD data were evaluated with data from colocated Sun photometers of the AERONET network [*Cheymol et al.*, 2009].

[20] Measured particulate mass concentrations (PM) are obtained from the French air quality monitoring network, handled by the French Environment and Energy Management Agency (ADEME). The mass concentrations analyzed within this study represent particles at the ground level with an aerodynamic diameter lower than 2.5 μm (PM2.5), measured continuously using a Tapered Element Oscillating Microbalance (TEOM). Drying of aerosol particles and evaporation of volatile components can lead to an underestimation of the PM values by the TEOM. The sampling sites are located at Lille, Calais (both in the North of France) and Marseille (South of France), all being densely populated and industrial areas that provide the main emission sources of anthropogenic aerosols. As for the AOD data, the model data are extracted for grid cells that are centered at the coordinates closest to the measurement location. Model PM2.5 concentrations are summed up from the smallest SS size bin, 5% of the second sea salt size bin (which is 0.5–5 μm), the two smallest DD size bins, and all bins of OM, BC, and SU. Note, that the PM2.5 data used here are daily mean values, which can smooth out possible local anomalies.

[21] The predictions of the GEMS aerosol model for the mass concentrations of sea salt and sulfate are compared to measurements from the EMEP (www.emep.int) network, as well as from the Mace Head GAW station for 2003. The selection criteria for observational data are: representativeness (e.g., marine sites only within 15 km from the coast or on islands), reliability (availability of sulfate data along with sodium for marine sites), uniform regional coverage, and long-term record. Most of the data are daily averages. For sulfate, either data from coastal stations with Na measurements or inland continental sites are used. Only data from sites below 1500 m amsl (meters above mean sea level) and thus within the continental or marine boundary layer are used. Those constraints significantly limit the availability of reliable data. There are no long-term monitoring measurements of OM or BC over Europe, only campaign-based data [*Yttri et al.*, 2007].

4. Case Studies

4.1. Air Pollution Event During the August 2003 Heat Wave in Europe

[22] This section presents a comparative analysis of GEMS DIRECT and ASSIM aerosol simulations with observation data for the severe heat wave of early August 2003 in western Europe. Conditions of persistent anticyclones characterized by high temperatures induced many processes (stagnation, photochemistry, forest fires in southern Europe), which led to unusually high aerosol loads [e.g., *Hodzic et al.*, 2006; *Tressol et al.*, 2008]. The episode ended around 15 August with the arrival of rainy conditions.

4.1.1. PM2.5, AOD, and Angström Exponent

[23] Remote sensing and in situ observations in the North of France showed that this region was among the areas which were affected by the severe heat wave. In this region, a maximum of aerosol loading was identified during August 2003 [*Kacenelenbogen et al.*, 2006]. For comparisons with the model simulations, AERONET data of daily mean AODs from the French sites in Lille, Dunkerque and Toulon are available. In addition, PM2.5 measurements are available

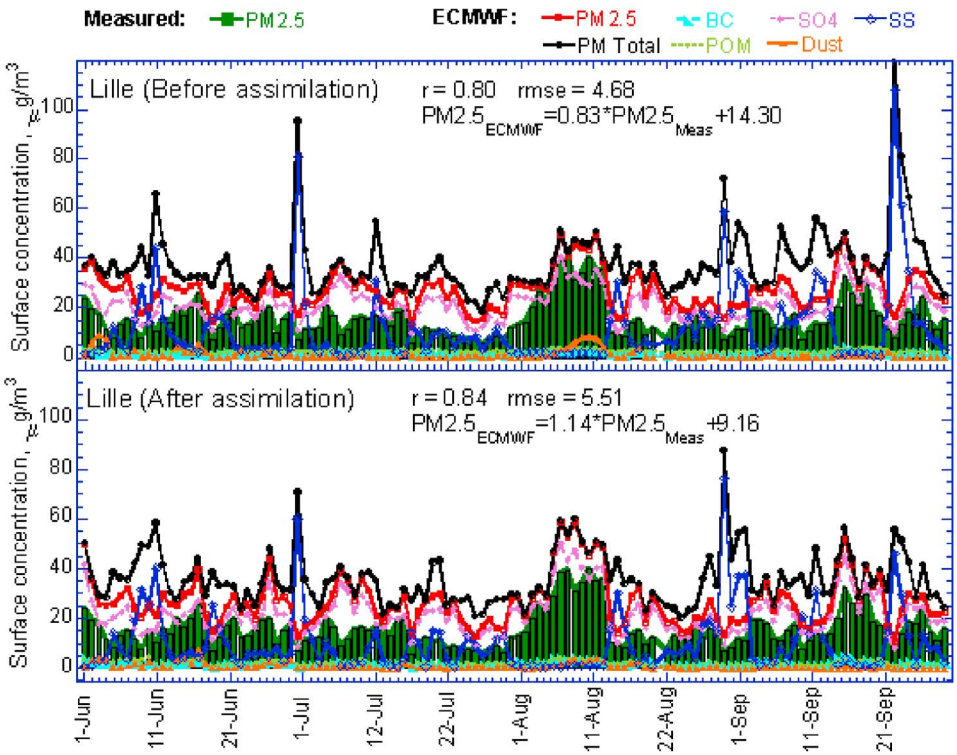

Figure 1. Time series of measured PM2.5 (green bars), simulated PM2.5 (red line), and simulated total PM (black line) for the period June to September 2003 for Lille. Also shown are the simulated concentrations of aerosol components from the GEMS-aerosol system. (top) DIRECT and (bottom) ASSIM version; r, rmse, and the regression equation are for PM2.5-measured against PM2.5-model.

for Lille, Calais (50 km from Dunkerque) and Marseille (60 km from Toulon). Note that the cities Dunkerque and Calais are in the same grid cell of the current model version, as are Marseille and Toulon. Dunkerque is surrounded by an important industrial center and our analysis (not shown) revealed that the PM2.5 concentrations at Calais are very well correlated with available PM10 concentrations at Dunkerque. In Lille, the AERONET and PM2.5 sampling stations are separated by about 5 km. The months June, July and September are included in this analysis for tracing the time evolution of the aerosol loading. In addition, part of the analysis is extended for the POLDER-2 operating period (April to October 2003).

[24] Figures 1, 2, and 3 present a comparison between the 24 h averaged PM2.5 concentrations sampled at the surface and the corresponding simulated (for both DIRECT and ASSIM) aerosol concentration for Lille, Calais and Marseille. The aerosol system picks up most of the day-to-day variability in the observed surface concentration of PM2.5 (compare green bars and red curve). In particular, the model represents well the relative increase from the average PM2.5 concentrations before the event to the average level during the heat wave period. The observed relative increase is distinct in Lille and Calais (PM2.5 increased twofold to threefold), but less pronounced in Marseille (increase with a factor around 1.5). The DIRECT simulation underestimates this relative increase. The ASSIM version agrees better with the observations, showing stronger relative increases at all three sites. During the heat wave event, model PM2.5 equals more or less total model PM with sulfate being the main component. The time periods before and after the event reveal higher fractions of coarse particles (difference model total PM and model PM2.5) in Lille and Calais than in Marseille. At all sites strong peaks of total PM concentration were simulated, when the model aerosol is made up almost completely by sea salt. It would be interesting to verify this, however, there are no respective observations of chemically resolved PM data available.

[25] Regarding the time period of the event, the DIRECT simulation overestimates PM2.5 in Lille and Calais and is very close to the observations in Marseille. The ASSIM simulation, however, introduces an additional overestimation, now also for Marseille. This is mainly due to increased SO_4 concentrations in the ASSIM version compared to the DIRECT run. Simulated BC concentrations show no distinct increase during the event, and OM concentrations increase only in Marseille in mid-July and in the beginning of August. Because the aerosol system assimilates total AOD, it cannot split between the individual aerosol species. If the DIRECT version, based on the emission databases and source functions, underestimates the assimilated parameter, the analysis reacts by increasing proportionally the mass of the individual aerosol species. The high level of sulfate in the DIRECT simulation results thus in the increase of sulfate by the assimilation. The simulated fractional contribution of BC and OM to PM2.5 are very low and so are the increases after assimilation.

[26] When looking at the whole period June to September 2003, the DIRECT simulation shows a systematic overestimation of PM2.5, higher in the North of France than in

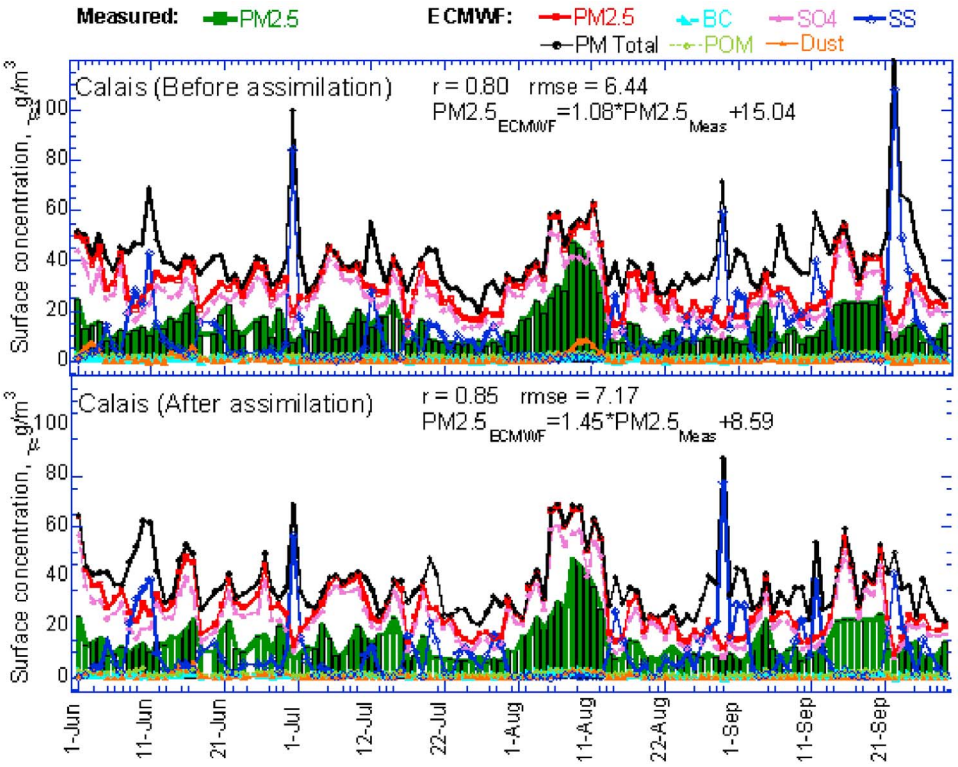

Figure 2. Same as Figure 1 but for Calais.

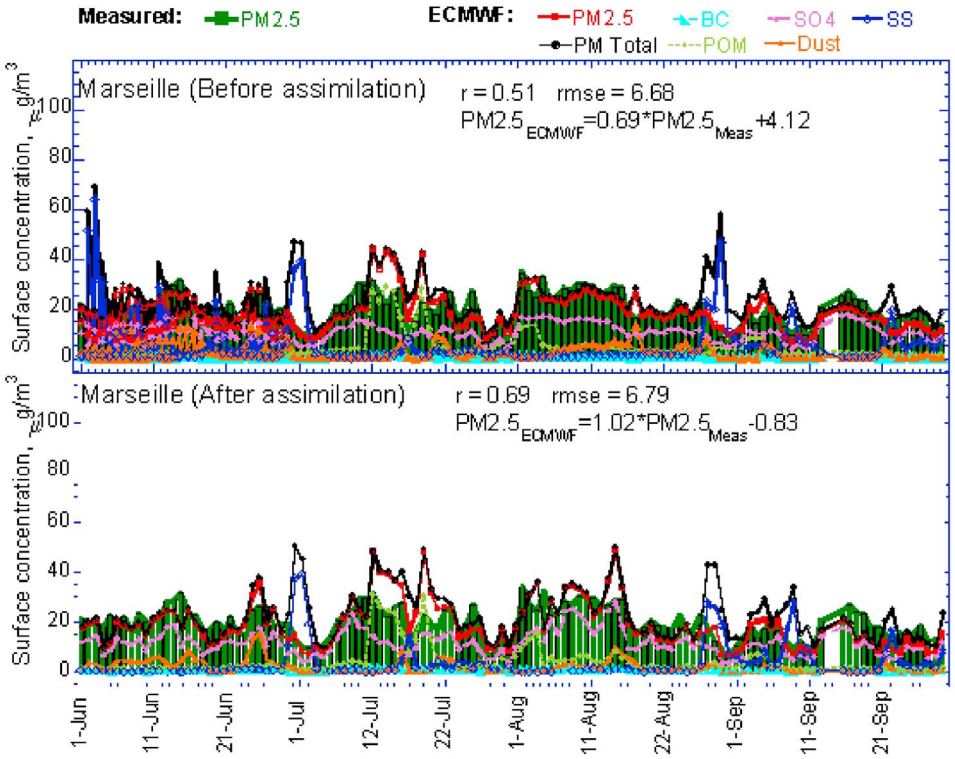

Figure 3. Same as Figure 1 but for Marseille.

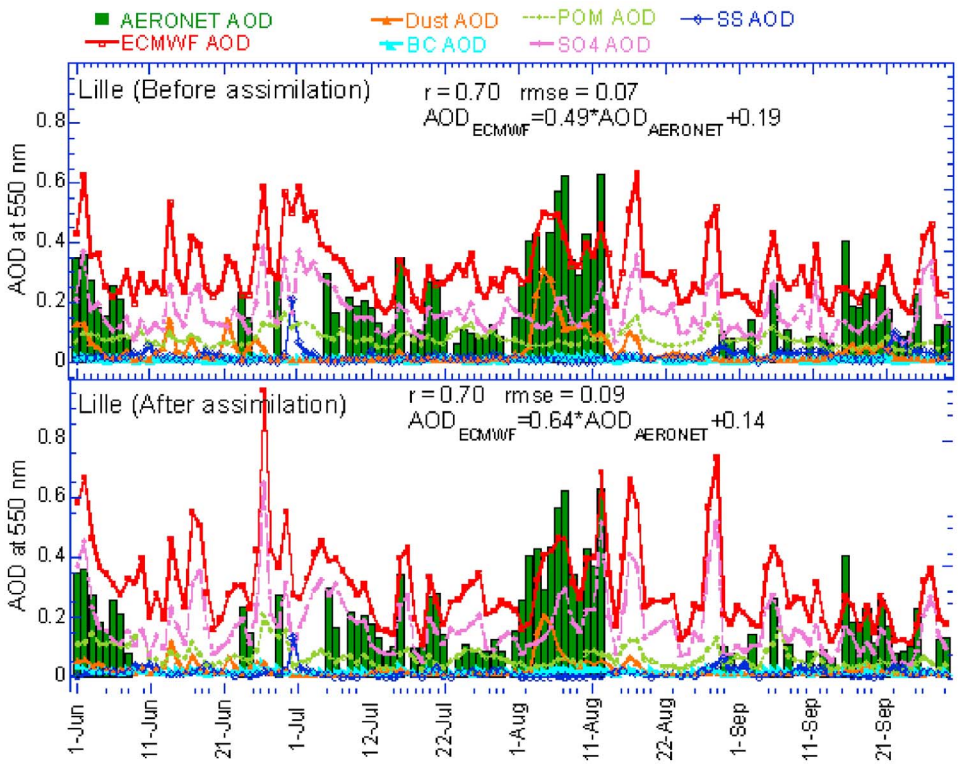

Figure 4. Time series of AERONET AOD (green bars) and simulated total AOD (red line) at 550 nm for June to September 2003 for Lille. Also shown are the simulated partial AODs of aerosol components from the GEMS-aerosol system. (top) DIRECT and (bottom) ASSIM version; r, rmse, and the regression equation are for AERONET-AOD against model-AOD. The gaps in AERONET AOD are due to the absence of measured values, for example, due to cloudy conditions.

Marseille, which is still present after the assimilation. The assimilation of MODIS AOD at 550 nm improves the correlation coefficients at all sites. The correlation coefficients after assimilation are 0.84 and 0.85 for Lille and Calais, respectively, and 0.69 for Marseille.

[27] Figures 4, 5, and 6 show time series of simulated (for both DIRECT and ASSIM) total and partial AODs compared to AERONET observations of AOD at 550 nm. The data are presented from June to September 2003 for Lille, Dunkerque/Calais and Toulon/Marseille. Likewise for the PM2.5 concentration, the aerosol system agrees reasonably well with the observed day-to-day variability of AOD (compare green bars and red curve). Regarding the whole period June to September 2003, the correlation coefficient is improved by the assimilation only in Toulon/Marseille (0.71 and 0.86 for DIRECT and ASSIM run, respectively). Lille and Dunkerque/Calais reveal unchanged correlation coefficients of 0.70 and 0.74, respectively. Observed AOD during the heat wave is high with some peaks greater than 0.6. The DIRECT simulation is in good agreement with the overall AOD level, however, there are mismatches between simulated and observed peaks (timing, both overestimation and underestimation), and especially at Toulon/Marseille the simulated AOD is too high in the early period of the event. The assimilation improves this picture only partly probably due to the same reasoning mentioned for the PM comparisons. On the other hand, the distinct peak of AOD on 13 August is well captured after the assimilation at all three sites. This is mainly due to increased model sulfate AOD (consistent with the increased sulfate PM2.5 mass mentioned above). Model partial BC and OM AOD values show no distinct increase during the event, for both DIRECT and ASSIM runs.

[28] Despite the relative agreement between the measured and the simulated AOD values, the overestimation of the simulated PM2.5 is pronounced. This PM2.5 overestimation most likely indicates issues with the vertical distribution of SO_4, which is the main component of simulated PM2.5. In cases of an agreement on AOD, the overestimation of PM2.5 can be due to a too high fraction of simulated boundary layer sulfate.

[29] The observed Angström exponent (440 to 870 nm; see Figure 7) reveals high daily variability in aerosol size, especially at Marseille. Concerning Lille and Dunkerque/Calais, this parameter is mostly higher than 1.0, and even up to 1.8, indicating rather small particles. In Toulon/Marseille there are more values below 1.0 and the Angström exponent shows some values between 0.2 and 0.5, and one negative value. A minor increase in simulated desert dust aerosol around 7 to 13 August (Toulon/Marseille also on 15 to 17 August) does not translate into a distinct variation of the Angström exponent. Some of these low values correspond to an increase in the model's dust component (e.g., on 25 and 26 June and 16, 21, and 22 July), but others do not.

[30] In Figure 8 we investigate the correlation of total AOD against PM2.5 concentrations, for measured and simulated

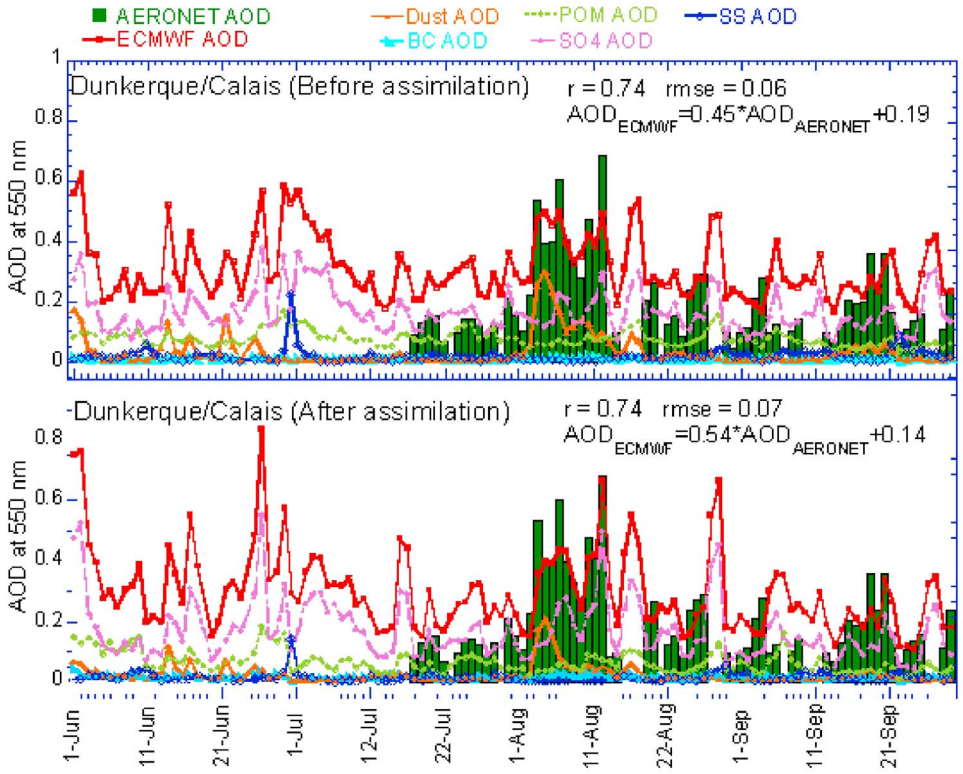

Figure 5. Same as Figure 4 but for Dunkerque/Calais.

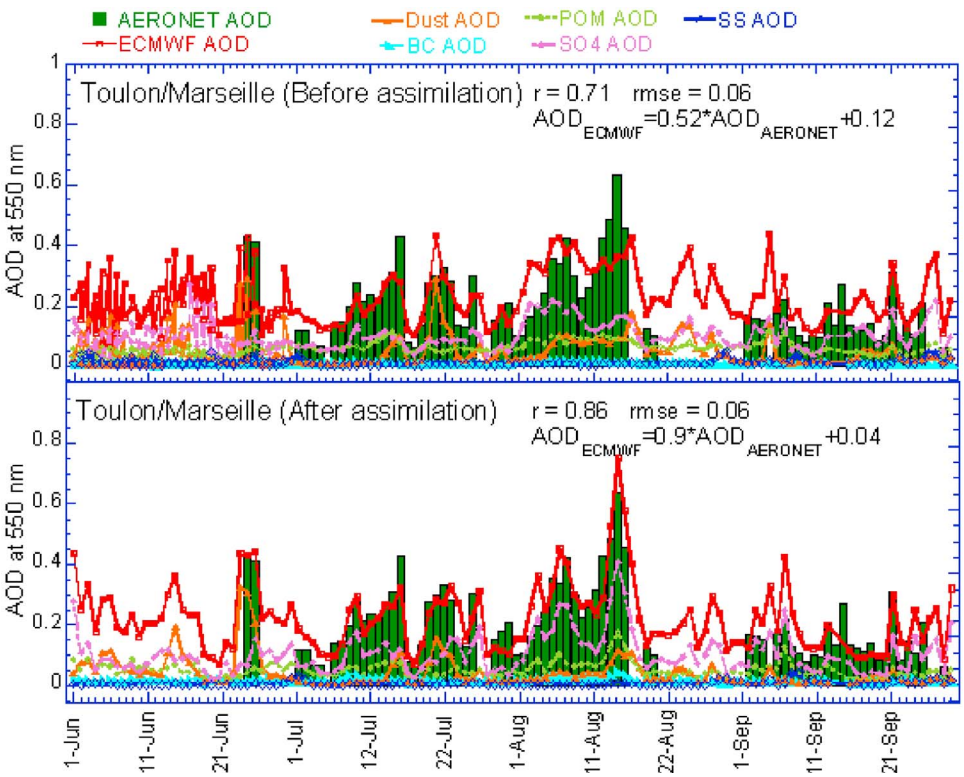

Figure 6. Same as Figure 4 but for Toulon/Marseille.

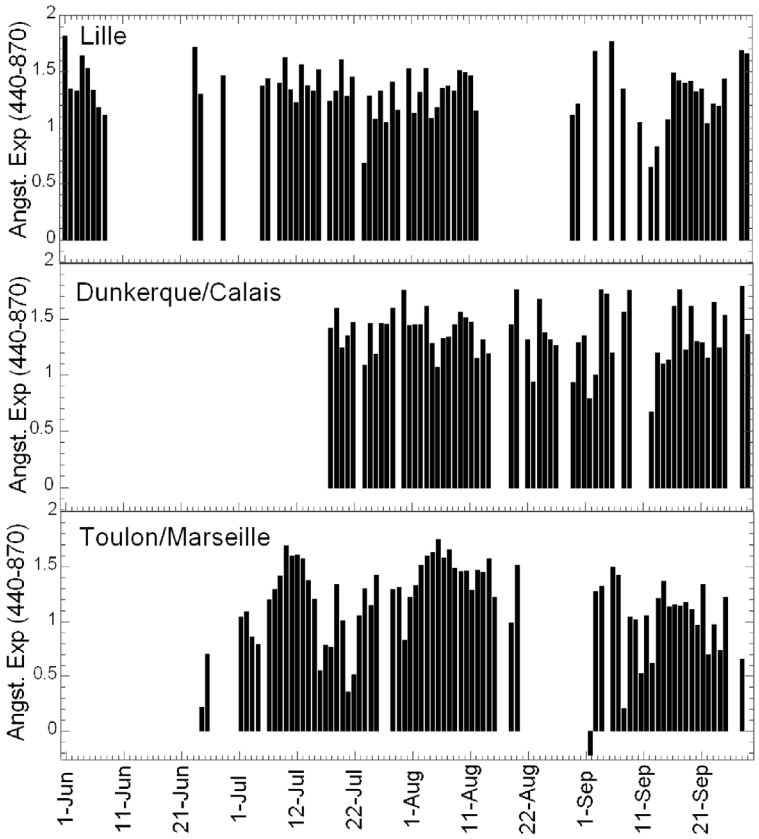

Figure 7. Time series of measured (AERONET) Angström exponent (440–870 nm) for June to September 2003 for Lille, Dunkerque/Calais, and Toulon/Marseille.

values. As total AOD is more easily measured (by ground-based or spaceborne instruments), this could enhance the PM2.5 database. The period end of July until mid-August is used, as it was identified by both observations and model as the period of elevated aerosol loading. During this period the model PM2.5 almost equals the total PM, providing a better consistency with total AOD. The data include all sites (Lille, Dunkerque/Calais, Toulon/Marseille), and the observed

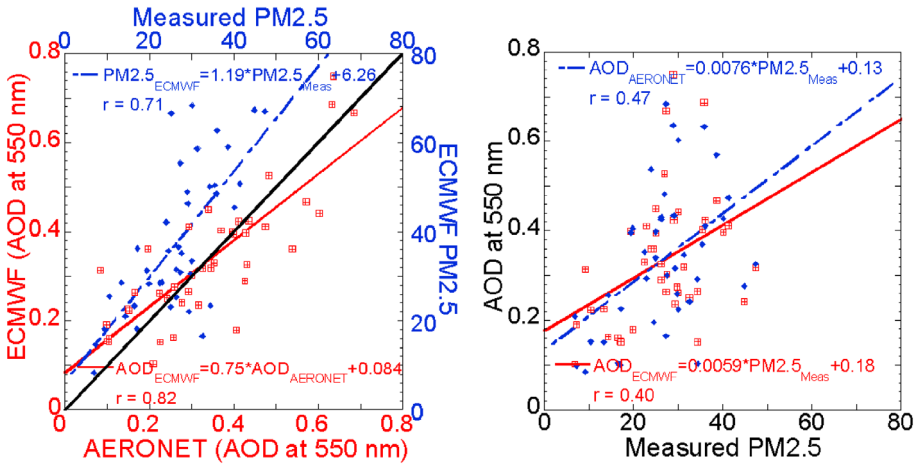

Figure 8. (left) Simulated (ECMWF) against measured (AERONET) AOD at 550 nm (red squares) and simulated against measured PM2.5 (blue diamonds); note that the scales are different. (right) Simulated AOD at 550 nm against measured PM2.5 (red squares) and measured AOD against measured PM2.5 (blue diamonds); the data include all sites (Lille, Dunkerque/Calais, and Toulon/Marseille) for the period of elevated aerosol loading from 31 July to 15 August 2003; simulated AOD and PM2.5 are for the ASSIM model run.

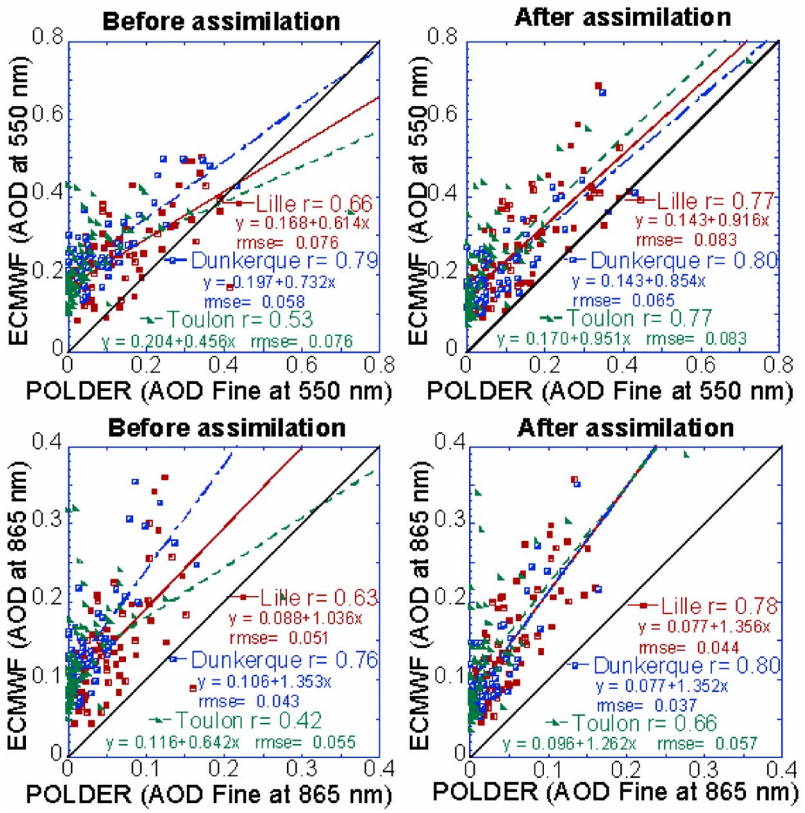

Figure 9. Total AOD simulated by the GEMS aerosol model against fine-mode AOD derived from POLDER-2 at (top) 550 nm and (bottom) 865 nm. Both (left) DIRECT and (right) ASSIM simulations are shown. The comparison is presented for the POLDER-2 operating period April to October 2003 for Lille, Dunkerque/Calais, and Toulon/Marseille. POLDER-2 and model data are at the same spatial resolution (1.125° grid).

AOD at 550 nm is from AERONET. Figure 8 (left) presents simulated (ASSIM version) against measured AOD ($r = 0.82$) and simulated against measured PM2.5 ($r = 0.71$). This good correlation is quite encouraging considering the low spatial resolution of the model and the local character of PM measurements. However, the correlation coefficient degrades for measured AOD against measured PM2.5 ($r = 0.47$; see Figure 8, right) and it degrades even stronger for the comparison of simulated AOD against measured PM2.5 ($r = 0.40$). This indicates the complexity and difficulties of modeling the conversion of aerosol species mass concentrations into optical properties, e.g., the vertical distribution of the aerosol species, their optical constants, or the spatial scales of the different parameters. A high correlation between PM2.5 (and its species composition) and total AOD would give information on the relationship between, on the one hand, mass and size, and on the other hand, optical properties of the aerosol species.

[31] Figure 9 presents for both DIRECT and ASSIM simulations total AOD against fine-mode AOD derived from POLDER-2 at 550 and 865 nm. The comparison is shown for the POLDER-2 operating period, separately for each site: Lille, Dunkerque/Calais, and Toulon/Marseille. The assimilation of MODIS AOD clearly improves the correlation coefficients at both wavelengths (550 and 865 nm), at all three sites. The positive offset in Figure 9 is due to the fact that model AOD is for total AOD and POLDER-2 AOD is for the fine-mode fraction AOD only. However, the assimilation of MODIS AOD reduces this high bias at all three sites.

[32] Figure 10 shows the correlations between simulated total AOD at 550 nm (for both DIRECT and ASSIM version) against fine-mode AOD derived from POLDER-2 and against total AOD from AERONET (both at 550 nm). The presented data are for coincident daily means from April to October 2003, and for all sites together (Lille, Dunkerque/Calais, and Toulon/Marseille). The graphs reveal that the assimilation improves quite similarly the model agreement with POLDER-2 fine-mode AOD and with AERONET total AOD. The model slightly overestimates the low and underestimates the high AOD values from AERONET. The comparison shows that the simulated total AOD has a slightly better correlation with AERONET total AOD than with POLDER-2 fine-mode AOD. Model total AOD reveals a distinct positive offset compared to the observations, more pronounced compared to POLDER-2 fine-mode AOD (DIRECT: 0.194, ASSIM: 0.155) than compared to AERONET total AOD (DIRECT: 0.143, ASSIM: 0.081). Although these offsets are reduced by the assimilation procedure, their origins need further investigation. Whereas a high bias of model total AOD compared to fine-mode AOD is logical, it is likely a combination of several points, causing the general positive offset. In addition to the general causes for a high bias of the ASSIM version, mentioned

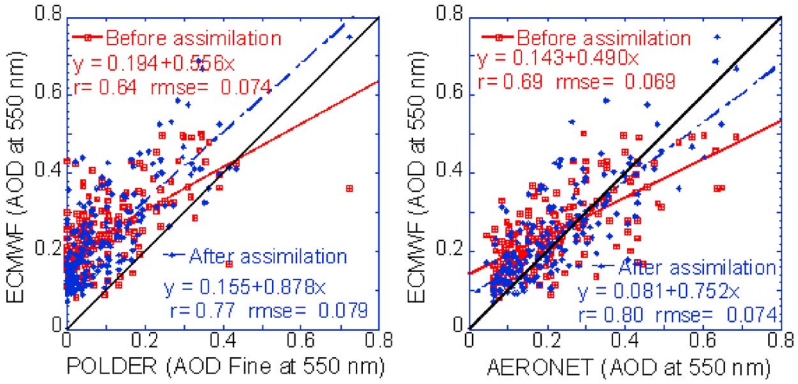

Figure 10. Total AOD simulated by the GEMS aerosol model against (left) fine-mode AOD derived from POLDER-2 and (right) total AOD derived from AERONET at 550 nm. Both DIRECT (red) and ASSIM simulations (blue) are given. Both graphs present coincident daily means for the same time period of April to October 2003 for all sites (Lille, Dunkerque/Calais, and Toulon/Marseille) together.

further above, the positive offset could be caused by an overestimation of sulfate, an incomplete (sources, time resolution) emission database, or shortcomings in the source function of sea salt and desert dust.

4.1.2. Elevated Sulfate Mass Concentrations During the Heat Wave

[33] Sulfate mass concentrations were enhanced during the summer heat wave period in central Europe in 2003 (see Figure 11). The nss (non sea salt) sulfate mass concentrations are shown for four EMEP stations–Illmitz (Austria, 47.7°N, 16.7°E), Montelibretti (Italy, 42.8°N, 12.4°E), Donon (France, 48.3°N, 8°E) and Peyrusse-Vielle (France, 43.4°N, 0.1°E)–encompassing an area of approximately 100,000 km^2. The concentrations roughly doubled during the heat wave period (Julian Days 213–230, 1 to 18 August), regardless of the absolute concentration differences between the sites. For instance, at the Montelibretti site, the sulfate mass concentration increased from approximately 6 to 16 μg/m^3. It is conceivable that the absence of precipitation was a major factor behind the increased sulfate concentration. Unfortunately, no organic or black carbon measurements are available within the EMEP network for this time period.

[34] The DIRECT model run captures the increase of sulfate mass concentration very well. The linear regression correlation coefficients between modeled and observed sulfate mass concentrations are in the range 0.50 to 0.67, indicative of a good general agreement (see Figure 12). The probability P of the null hypothesis that the correlations are

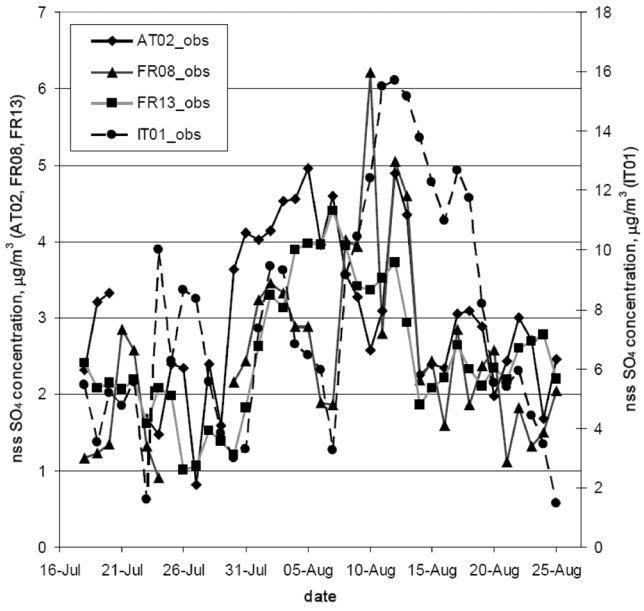

Figure 11. Time series of observed non sea salt sulfate mass concentration at 4 EMEP stations during summer 2003 (17 July to 26 August, daily averages from 6 h values). The heat wave period was between Julian Days 213 and 233 (1 to 21 August). AT02, Illmitz, Austria; FR08, Donon, France; FR13, Peyrusse-Vielle, France; IT01, Montelibretti, Italy (see text).

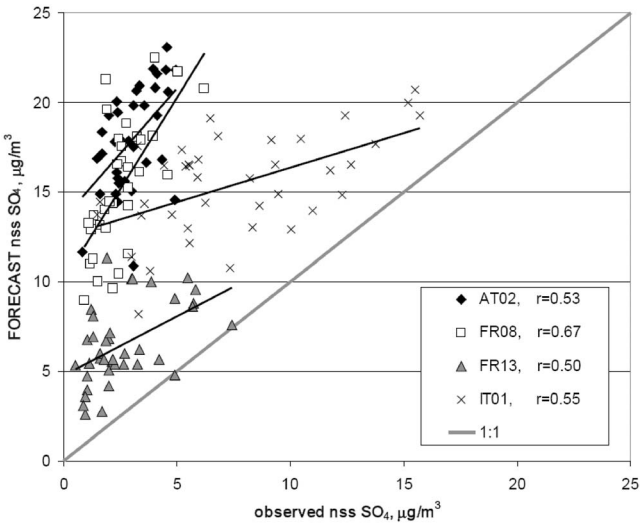

Figure 12. Correlation and linear regression between observed and simulated (DIRECT simulation) sulfate mass concentrations at four EMEP stations (see text) for 17 July to 26 August 2003.

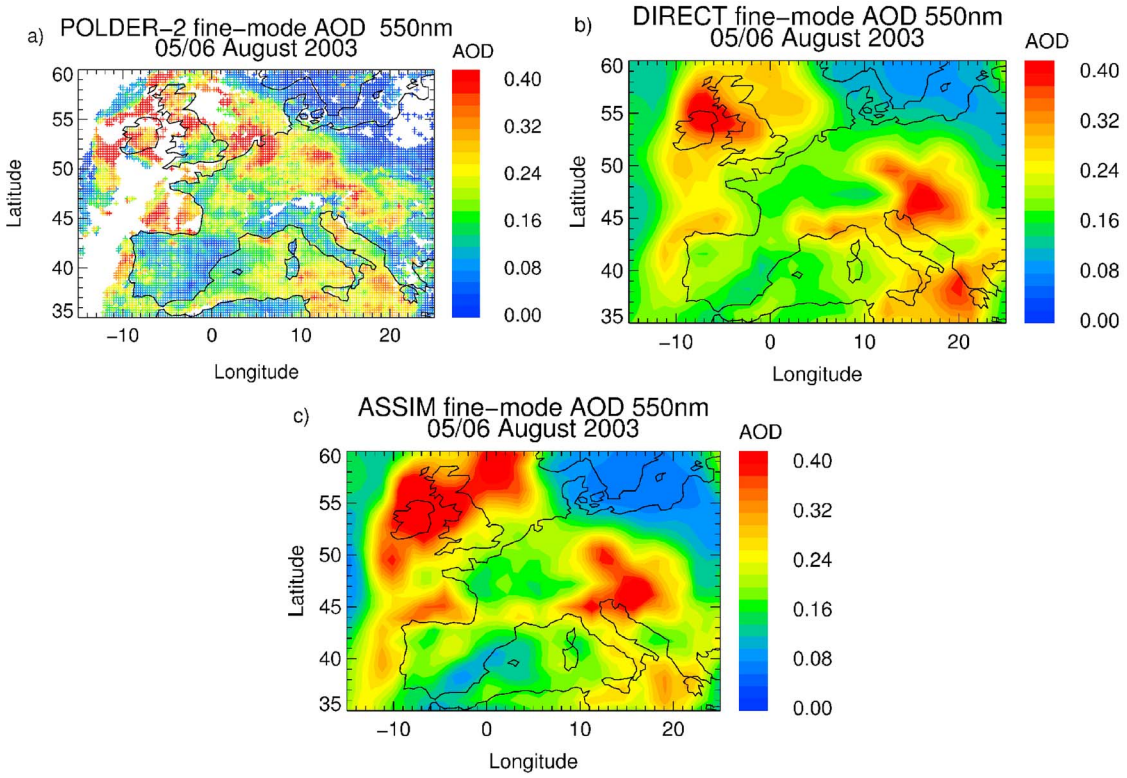

Figure 13. Mean fine-mode AOD over Europe for (a) POLDER-2 observations extrapolated to 550 nm, (b) DIRECT, and (c) ASSIM model simulations at 550 nm; for the time period 5 to 6 August 2003, covered by POLDER-2 observations (time interval 0900 to 1500 UT each day); note that model fine-mode AOD is the sum of the partial AODs of BC, OM, and SU.

accidental is below 0.01; that is, the correlations are significant. However, the regression analysis indicates a significant overestimation of aerosol sulfate by the model, which can be attributed either to inadequate emission inventories of SO_2, too efficient and rapid conversion of SO_2 to SO_4 in the sulfate aerosol scheme, too weak dry deposition of SO_2, or discrepancies in the aerosol vertical profile. The assimilation of MODIS AOD does not improve significantly the simulation of the mass concentrations.

4.1.3. Portuguese Fire Aerosol Over Middle Europe

[35] The dry conditions of summer 2003 led to many wild fires in Southern Europe, in particular in Portugal between 3 and 8 August 2003 [*Hodzic et al.*, 2007]. These wild fires provide the opportunity to investigate the aerosol model capability to simulate the spatial transport of the fire plume aerosols.

[36] The graph of POLDER-2 mean fine-mode AOD at 550 nm (see Figure 13a) shows elevated fine-mode aerosol on 5 and 6 August 2003 over the Atlantic next to Portugal and France, the British Isles, the North Sea, the Netherlands, parts of eastern Europe from eastern Germany to the Balkan countries and over the eastern part of the Mediterranean Sea. That the northwestern part of Europe was affected by smoke aerosols has been shown by several authors [*Hodzic et al.*, 2006, 2007; *Tressol et al.*, 2008]. *Hodzic et al.* [2006] presented a passive tracer study (taking into account the emission of primary aerosols due to forest fires and their subsequent atmospheric transport), which revealed that the tracer was transported from Portugal via the British Isles, and the North Sea to the Benelux area, within an altitude of 3 to 4 km. *Tressol et al.* [2008] modeled the CO emissions of the Portuguese fires and their spatial transport, showing that the CO plume on 6 August 2003 and at 2.5 km altitude stretched from Portugal to the British Isles, the North Sea and the Benelux area.

[37] The mean fine-mode AOD simulations at 550 nm for the period 5 to 6 August 2003, for both DIRECT and ASSIM simulations, are compared to POLDER-2 fine-mode AOD at 550 nm in Figures 13a–13c. Note, that model fine-mode AOD is approximated by the sum of the partial AODs of BC, OM, and SU. These partial AODs are available only at 550 nm, which is not an original wavelength of the POLDER-2 AOD product. Therefore, POLDER-2 AOD has to be adjusted to the model and the fine-mode AOD is extrapolated to 550 nm using the Angström exponent of the fine-mode AODs at 670 and 865 nm. It has to be mentioned that the accuracy in the derived POLDER-2 AOD and AOD spectral dependence over land and over ocean can be different, which can be reported in differences in the extrapolated AOD values. The accuracy of the AOD spectral dependence and thus of the extrapolated AOD is decreasing over land for low aerosol loadings.

[38] The DIRECT simulation agrees reasonably well with the general pattern of areas of elevated fine-mode aerosol observed by POLDER-2, however, missing the elevated aerosol over the Netherlands and its adherent part of the North Sea, overestimating the AOD over northern Italy, the south of France, and over the Iberian peninsula, and underestimating

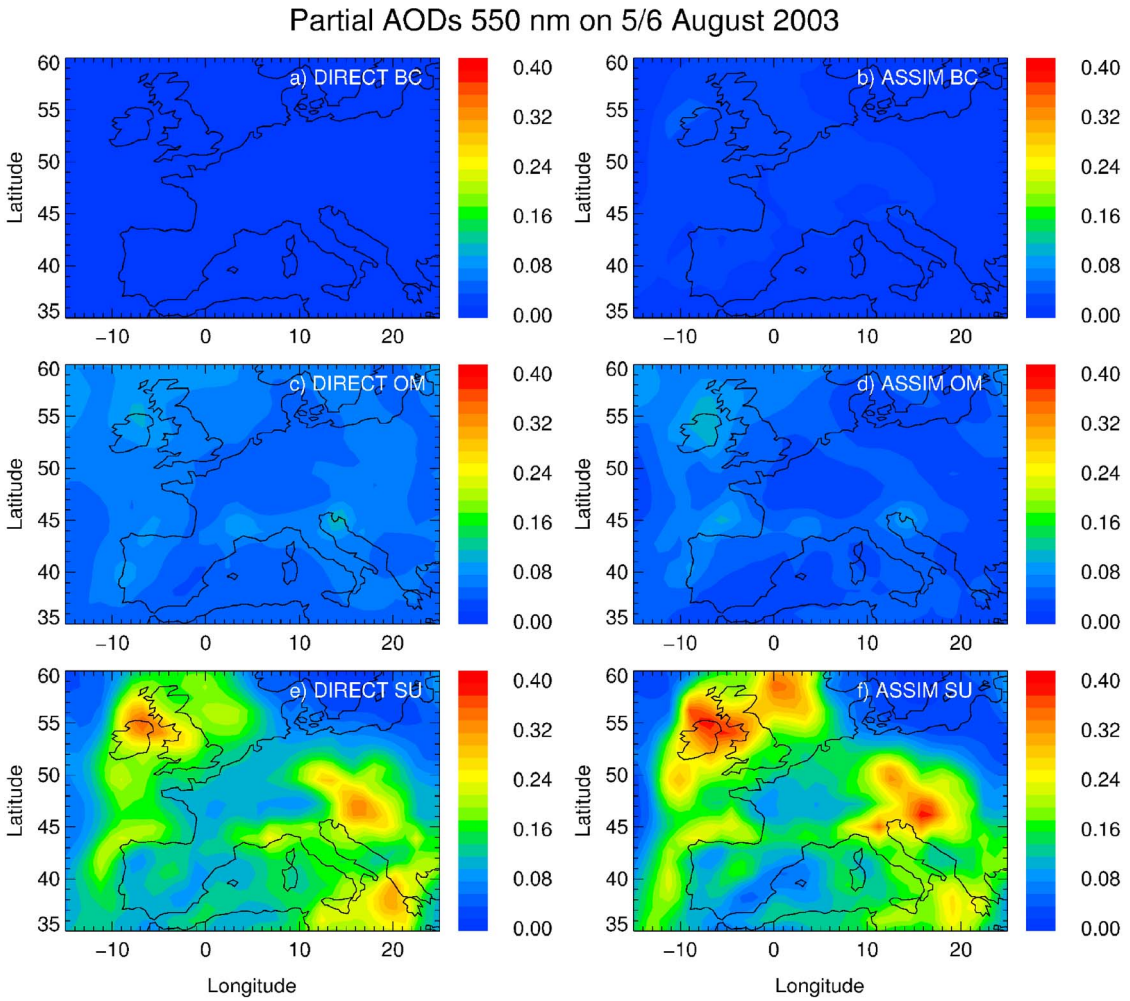

Figure 14. Mean partial AODs at 550 nm of (a, b) BC, (c, d) OM, and (e, f) SU, for both DIRECT (Figures 14a, 14c, and 14e) and ASSIM (Figures 14b, 14d, and 14f) simulations, for the period of 5 to 6 August 2003 covered by POLDER-2 observations (time interval 0900 to 1500 UT each day).

the fine-mode AOD over the Atlantic next to Portugal and France. The assimilation increases the AOD over most of the areas of the DIRECT simulation with elevated fine-mode AOD. There is now a clear overestimation of AOD over the British Isles, the part from Eastern Germany to the Balkan countries and northern Italy. The assimilation improves the agreement over the Atlantic next to Portugal and France, eastern Spain, the south of France, the Baltic Sea, and the eastern Mediterranean Sea. On the contrary, the assimilation is also not able to reproduce the observed peak over the Netherlands and the adherent part of the North Sea.

[39] Therefore, it is important to look at the mean partial AODs of BC, OM, and SU at 550 nm in Figure 14, for both DIRECT and ASSIM simulations. Within the simulations, only SU contributes significantly to the total fine-mode AOD and the assimilation increases the levels of each of the three aerosol species. OM plays a minor part and BC only a marginal one, although in a smoke plume these two species should be distinctly stronger represented. The discrepancies may result from the smoothed 8 day resolution of the emissions, which does not capture the strength of individual fires. Also, a parameterization of the injection height of fire-produced aerosol is required to properly represent long-range transport of aerosols from fire emissions.

4.2. Saharan Dust Event March 2004

[40] In early March 2004, a cold air outbreak from Europe to Africa caused a major dust storm over large parts of western Africa [*Knippertz and Fink*, 2007]. Subsequently, the cold air fanned out across the Sahara, diverging over subtropical regions and the Atlantic Ocean. The DIRECT and ASSIM simulations of AOD, Angström exponent and coarse-mode AOD are compared to data retrieved from satellite (SEVIRI) and ground-based data (AERONET, Brewer spectrophotometer). MODIS images onboard Terra and Aqua satellites from 3 to 6 March 2004 (Figure 15) illustrate this dust event. On 3 March, an arc of dust was formed that swept over the Canary Islands. On 5 March, the dust reached the Cape Verde Islands and the shores of western Europe.

[41] Figure 16 illustrates that the model run with data assimilation simulates very well the spatial distribution of the dust plume. However, compared to SEVIRI AOD data, the model both underestimates and overestimates AOD in

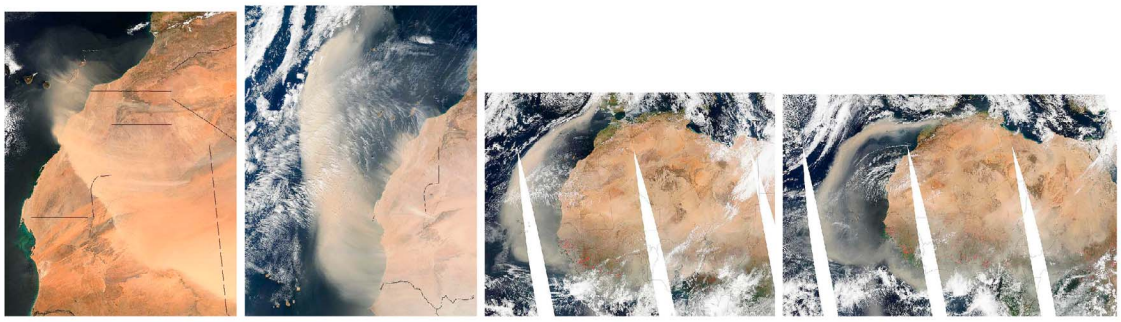

Figure 15. Dust plume observed by MODIS on Terra and Aqua satellites. From left to right: 3 March 2004, 1415 UT (Terra); 4 March 2004, 1155 UT (Terra); 5 March 2004, 1405 UT (Aqua); 6 March 2004, 1450 UT (Aqua).

parts of the dust plume over the ocean (see Figure 16c). Especially in the core of the plume, the model underestimates the observed AOD. It should be noted that part of this difference can be attributed to the uncertainty of the SEVIRI AOD retrieval [see *De Paepe et al.*, 2008]. However, MODIS AOD graphs of 5 and 6 March 2004 also showed AOD values distinctly higher than 2 for the core of the dust plume [see *Benedetti et al.*, 2009, Figure 7c]. That the assimilation of MODIS AOD improves distinctly the performance can be seen in Figure 16d, revealing an improvement also for regions void of MODIS AOD data, such as over bright surfaces (e.g., Niger, Nigeria, and Chad).

[42] Graphs of the correlation between simulated AOD at 670 nm and SEVIRI AOD at 630 nm are shown in Figure 17 for 4, 5 and 6 March 2004, for both DIRECT and ASSIM simulations, and averaged over the time interval 1200–1500 UT. Data pairs are taken from the common grid cell area 0° to 40.5°N and 4.5° to 36°W. The higher-resolution data of SEVIRI was scaled to the model grid. Note, as SEVIRI AOD are only available over ocean, no AOD over land is included in these correlations. The assimilation clearly improves the agreement with observed SEVIRI AOD over the whole AOD range, in particular the linear correlation coefficient r is improved, up to 0.76 (5 March 2004, 1200–1500 UT; see Figures 17c and 17d). Whereas the DIRECT simulation distinctly underestimates the observed AOD, this low bias is clearly reduced in the ASSIM version, both at low and high AOD values.

[43] As the GEMS and SEVIRI common grid cell area covers areas both affected and unaffected by the dust plume,

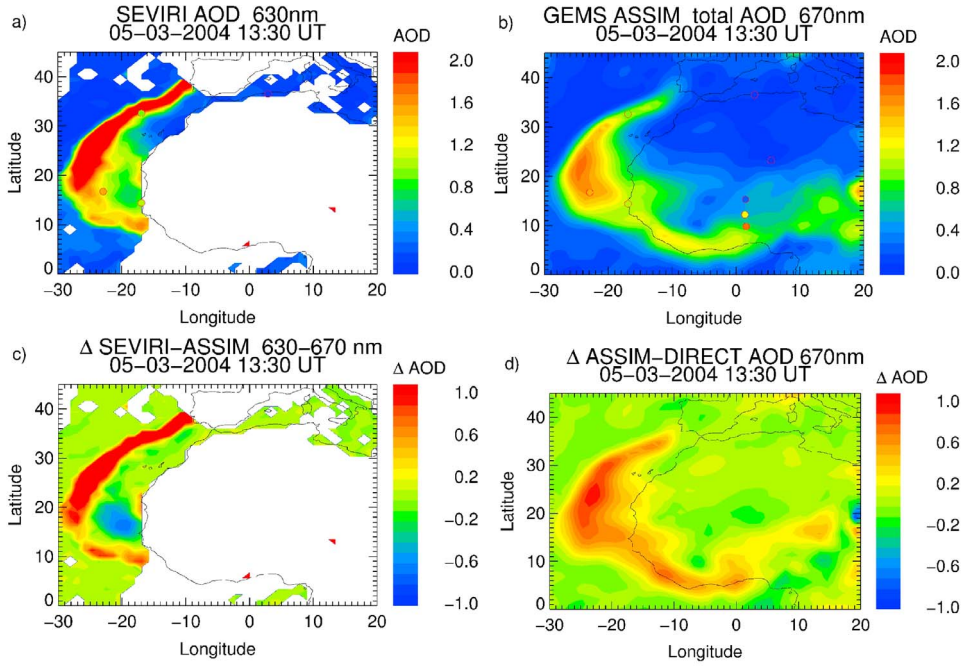

Figure 16. (a) SEVIRI-AOD at 630 nm, for 5 March 2004, 3 h average 1200–1500 UT; color-filled circles represent AOD from ground-based measurements. (b) GEMS-AOD (ASSIM) at 670 nm, for 5 March 2004, for the time interval 1200–1500 UT; color-filled circles represent AOD from ground-based measurements. (c) AOD difference graph SEVIRI minus ASSIM. (d) AOD difference graph ASSIM minus DIRECT.

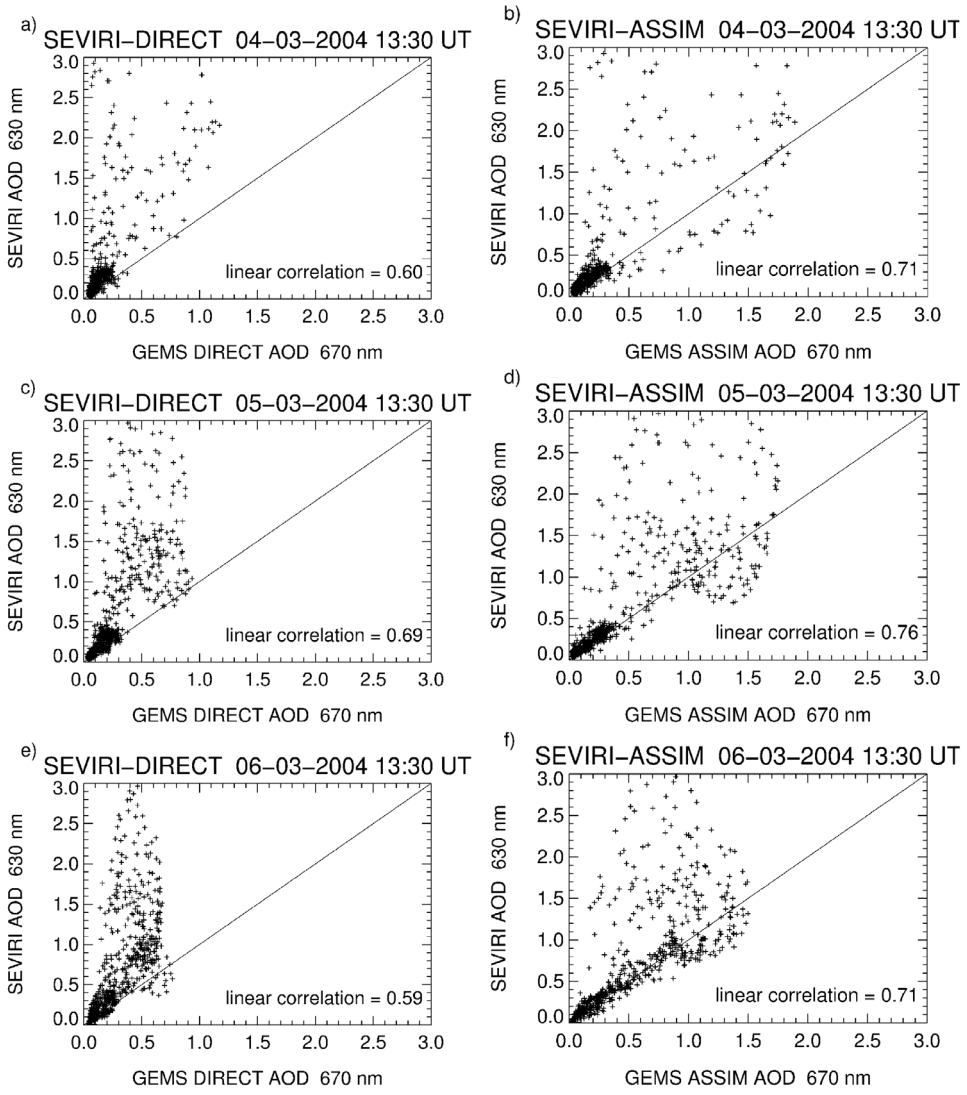

Figure 17. Correlation of total AOD between SEVIRI at 630 nm and both (a, c, and e) DIRECT and (b, d, and f) ASSIM simulations at 670 nm, for the 4th (Figures 17a and 17b), 5th (Figures 17c and 17d), and 6th (Figures 17e and 17f) March 2004, always for the time interval 1200–1500 UT; data pairs are for the area 0°N–40.5°N and 4.5°W–36°W and only over ocean; the linear correlation coefficients are given in the graphs; the straight black line is the 1:1 line.

and thus areas of dominantly higher and lower AOD, respectively, the correlation calculations are additionally done separately for the AOD ranges above and below 0.5. Such calculations were done for all 3 h intervals of 4, 5 and 6 March between 0600 and 2100 UT (time when SEVIRI AOD is retrievable). Whereas the mean correlation coefficient for the ASSIM simulations is 0.64 ± 0.13 (DIRECT 0.54 ± 0.14) for the whole AOD range, the correlations for AOD values below 0.5 are slightly weaker (ASSIM mean: 0.57 ± 0.16; DIRECT mean: 0.51 ± 0.15). The correlations for the range 0.5 to 3.0 are very low (ASSIM mean: 0.15 ± 0.15; DIRECT mean: 0.1 ± 0.08). Statistically, all correlations are significant; that is, the probability P of the null hypothesis that the correlations are accidental is below 0.01. This indicates that the assimilation is very efficient for the low AOD values, but less for very high AOD values. The assimilation reduces the model low bias at high AOD values, but less the scatter.

[44] Time series of AOD at four AERONET sites (Agoufou, Capo Verde, Dakar, El Arenosillo) and one Brewer station (Funchal, Madeira islands) were selected to illustrate both the performance of the GEMS aerosol model simulating a Saharan dust event and the impact of the assimilation of MODIS AOD (see Figure 18). At Agoufou, a maximum of AOD was present on 4 March, at Dakar, Capo Verde and Funchal on 5 March, and at the more distant station of El Arenosillo in southeastern Spain, the peak was observed on 6 March. The increase of AOD and the timing of the peaks are well represented by both the DIRECT and the ASSIM simulation, and both versions correctly assign almost all of the total AOD to desert dust during the event. The DIRECT simulation underestimates total AOD at all observation sites whenever dust dominates total AOD, in particular the peaks. Considering the closeness of Agoufou and Dakar to the dust origin, this suggests that the model underestimates the

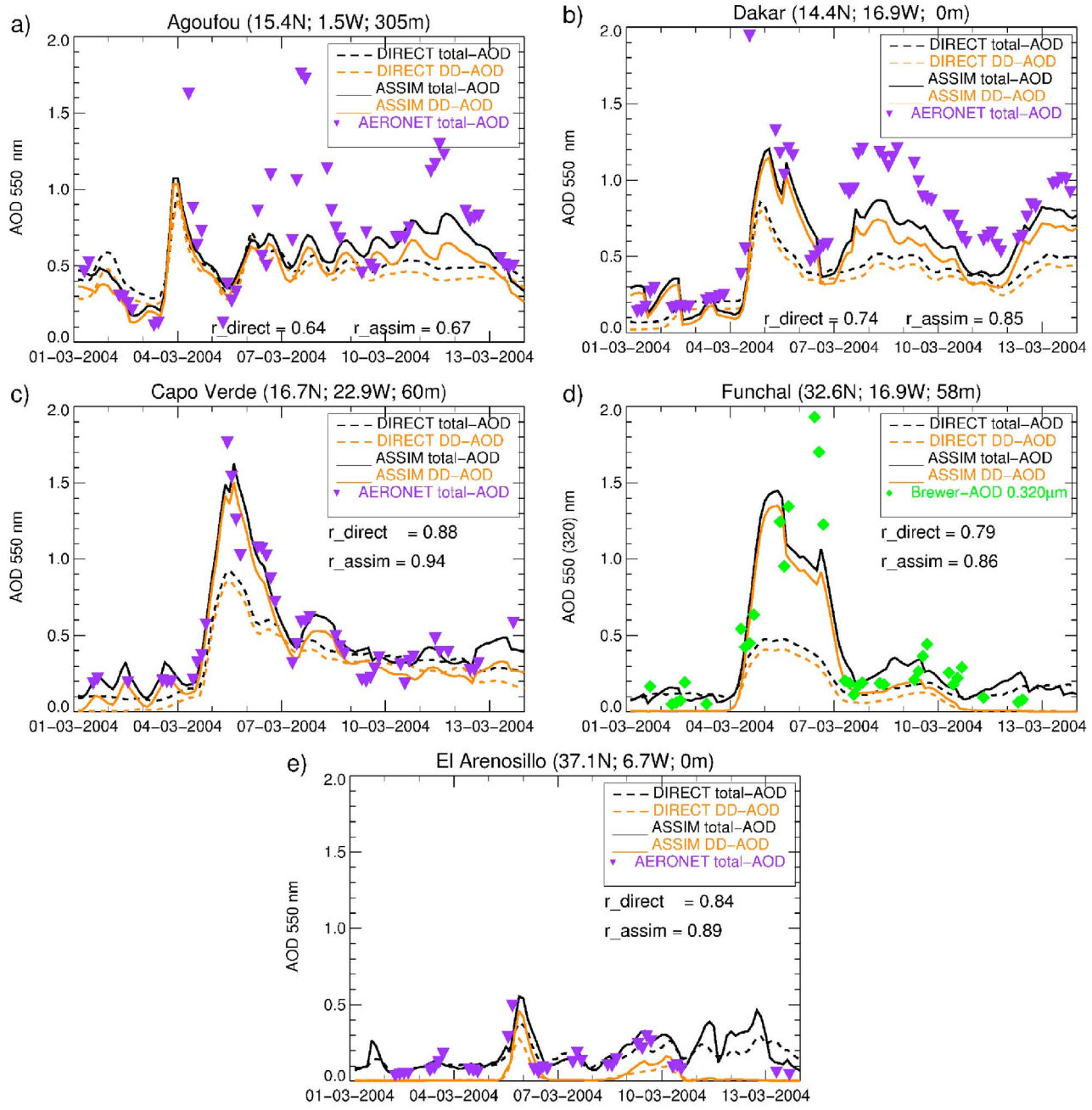

Figure 18. Time series of AOD for March 2004 observed at (a, b, c, and e) four AERONET sites (total AOD at 550 nm, violet triangles, Agoufou, Capo Verde, Dakar, El Arenosillo), and (d) one Brewer station (total AOD at 320 nm, green diamonds, Funchal); simulation data for total AOD at 550 nm (DIRECT, dashed black line; ASSIM, solid black line), and DD AOD at 550 nm (DIRECT, dashed orange line; ASSIM, solid orange line); the linear correlation coefficients for both model versions are given in the graphs.

intensity of the emissions. The assimilation of MODIS AOD improves the model performance. Differences between model and observations are distinctly reduced and the peaks are more pronounced.

[45] The correlation coefficients between observations and model reveal the highest correlations after assimilation at Capo Verde and El Arenosillo (0.94 and 0.89, respectively), whereas Agoufou, the station closest to the dust origin, shows the lowest correlation (0.67). At all stations the assimilation improves the correlation. All correlations are statistically significant. Note, that in Funchal the AOD is measured at 320 nm. Because of the spectral dependency of light scattering and absorption by aerosols, a positive bias between AOD at 320 and 550 nm can be expected, which should however be small in the case of mainly coarse dust aerosols.

[46] Both simulations overestimate the Angström exponent (see Figure 19), an indicator of aerosol size, at the sites of Agoufou, Dakar and Capo Verde, whereas at the more distant station El Arenosillo the Angström exponent is better

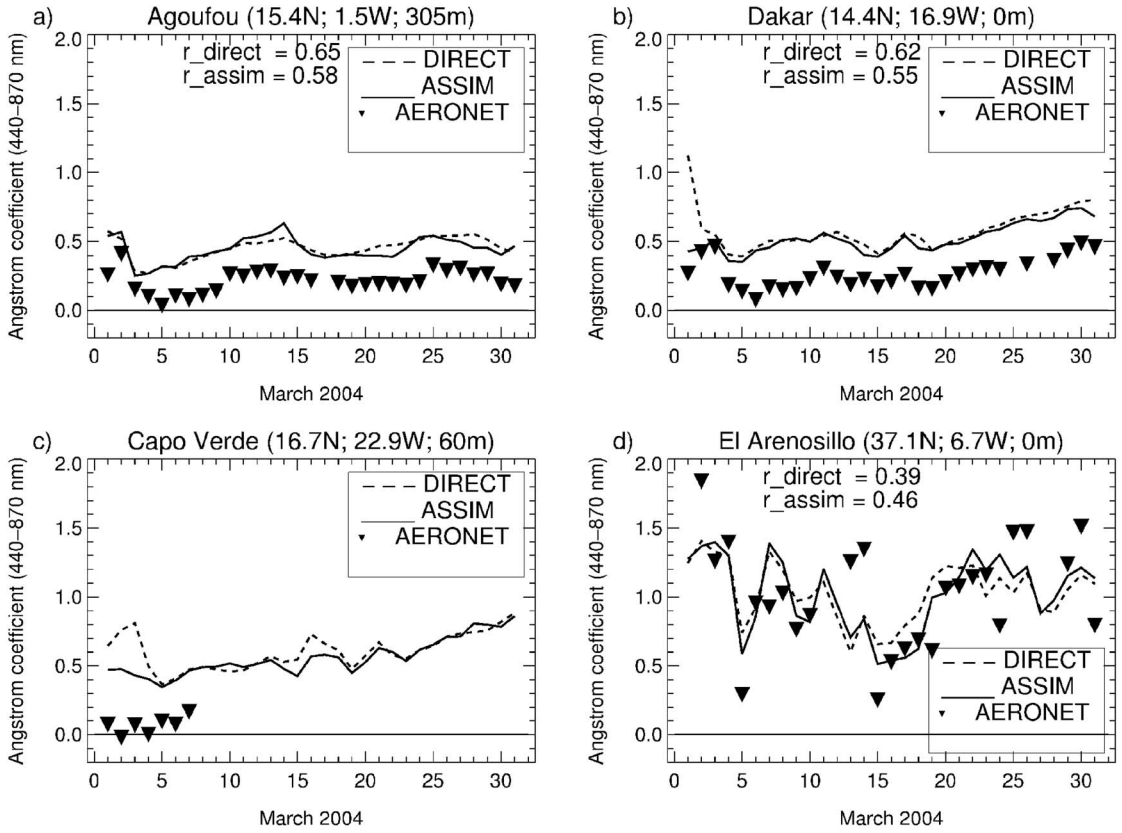

Figure 19. Angström exponent for March 2004 at (a) Agoufou, (b) Dakar, (c) Capo Verde, and (d) El Arenosillo; AERONET data (black triangles) against DIRECT (dashed black line) and ASSIM (solid black line) simulations.

reproduced, with a slight overestimation the day of the dust arrival. No major differences are detected in the performance to reproduce the Angström exponent between the two model runs, revealing that the assimilation has little impact on correcting the model in terms of dust size distribution. The linear correlation coefficients range from r = 0.39 at El Arenosillo for the DIRECT simulation, to r = 0.65 at Agoufou, also for the DIRECT simulation. The assimilation improves r only for El Arenosillo. The corrections to the model through the assimilation of total AOD at 550 nm are done in terms of total aerosol loading and not in terms of size distribution. Furthermore, the overestimation of the Angström exponent in Agoufou, Dakar and Capo Verde, and a better performance in El Arenosillo reveal that the fine-mode aerosol is overestimated by both model versions.

[47] In addition, Figure 20 displays the coarse-mode AOD in Agoufou, Capo Verde, Dakar and El Arenosillo, retrieved from both AERONET sky measurements and the model for March 2004. Compared to Figure 18, it is obvious that in Agoufou, Capo Verde and Dakar the coarse mode dominates total AOD. In El Arenosillo, more distant to the dust origin, the coarse mode is less important, although there are distinct periods when the Angström exponent is below 0.4, indicative of coarse particles. Whereas the DIRECT simulation mostly underestimates the coarse-mode AOD, this parameter is overcorrected by the assimilation, especially in Capo Verde. Note, that model coarse-mode AOD is the sum of partial DD and SS AOD. Likewise for the Angström exponent, the linear correlation coefficients are not high (between r = 0.49 at El Arenosillo for DIRECT, and r = 0.69, for ASSIM at El Arenosillo). Again, the assimilation improves r only for El Arenosillo. The system assimilates total AOD and can therefore not split between coarse and fine particles. If the DIRECT version underestimates total AOD, the analysis reacts by increasing the mass of both fine- and coarse-mode aerosols. Because of the aerosol optical properties used for calculating the AOD (see section 2), this results in an overestimation of the coarse mode AOD, as illustrated in Figure 20.

4.3. Periods of High and Low Sea Salt Aerosol

[48] Sea salt events are normally associated with high wind speed periods lasting for several days. At Mace Head, cases with high wind speed are most often observed when low-pressure systems are advected from the Atlantic Ocean. However, low-pressure systems are connected with cloudiness. Therefore, the number of events when observational AOD data are available is very low. For this study, sea salt cases were separated into winter and summer events, as there were distinct differences between them.

4.3.1. Winter Sea Salt Events

[49] During winter, low-pressure systems in the North Atlantic are normally deeper compared to summer, which means that higher wind speeds are observed. Consequently, more sea salt is generated across the entire aerosol size range [*O'Dowd and Smith*, 1993; *Yoon et al.*, 2007]. Two cases

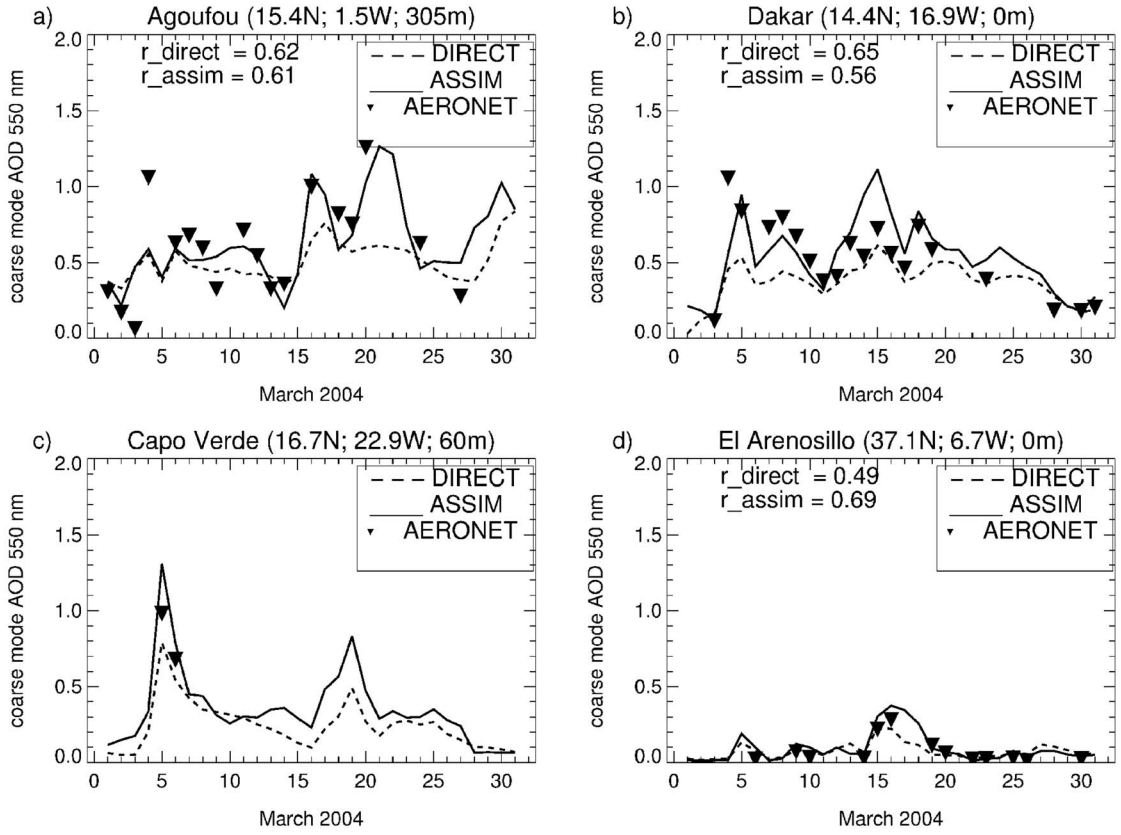

Figure 20. Coarse-mode AOD for March 2004 at (a) Agoufou, (b) Dakar, (c) Capo Verde, and (d) El Arenosillo; AERONET data (black triangles) against DIRECT (dashed black line) and ASSIM (solid black line) simulations; note that model coarse-mode AOD is the sum of partial DD and SS AOD.

were selected for the winter period in 2003. The first one occurred during 14 and 17 January 2003 (Julian Days 14–17), the other one during 3 to 4 November 2003 (Julian Days 307–308; see Figure 21). During both events wind speed was above 15 m/s as observed at the coastal research station in Mace Head, with up to 20 m/s as an hourly average. These two cases were selected not only because of observed high wind speed, but also due to sufficiently long periods of clear skies, providing reliable observational AOD data from a Precision Filter Radiometer [*Wehrli*, 2004].

[50] Measured sea salt concentration in bulk aerosol samples during these two events was 24 and 19.2 $\mu g/m^3$ for the January and November event, respectively. These were not the highest concentrations measured during the entire year of 2003, but were among the highest 5% of values. Figure 21 shows time series of observed wind speed, simulated (DIRECT run) total and sea salt AOD, as well as observed AOD during January and November 2003. The assimilation of MODIS AOD does not change significantly the SS AOD simulations (the same is true for the summer events). Simulated total AOD and partial SS AOD values range from 0.02 to 0.6, with peaks up to 1.1. During the events the total IFS AOD is dominated by sea salt and model AOD generally overestimates the observed total AOD. Around 20 January 2003, the observed AOD is more distinctly overestimated. A similar overestimation was demonstrated by *Morcrette et al.* [2008]. There are a few more noticeable mismatches between IFS AOD data and wind speed (e.g., around Julian Days 24–26, 30, 318). Given the time lag between wind speed and the AOD needs to build up both in the real atmosphere and in the model, a significant mismatch can occur, especially in the case of changing wind speed and direction. This was the case in particular on 20 January 2003. The effect of stable wind speed on observed AOD is discussed in detail by *Mulcahy et al.* [2008], who demonstrated a clear power law relationship between stable wind speed and AOD.

[51] Unfortunately, no good satellite data exist for those cases, due to the season (satellites are "blind" in northern latitudes during winter) and cloudiness and are thus not presented here. However, the composite MODIS AOD image for the November event matches in general the ground-based AOD with values in the range 0.1 to 0.3 (http://neo.sci.gafc.nasa.gov/).

4.3.2. Summer Sea Salt Events

[52] For the summer 2003, two sea salt events were selected: 17 to 24 May (Julian Days 137–144) and 2 to 9 June (Julian Days 153–160; see Figure 22). These events were quite different from the winter ones considering AOD. The wind speed for these events was somewhat lower (10–15 m/s) when compared to the winter cases. The simulated (DIRECT run) total and partial SS AOD follows the wind speed variation more closely than during the winter period. Model total and partial SS AOD values are lower than in the winter cases (total AOD values range from 0.1 to 0.4, with peaks up to 0.85). Due to the lower wind speed

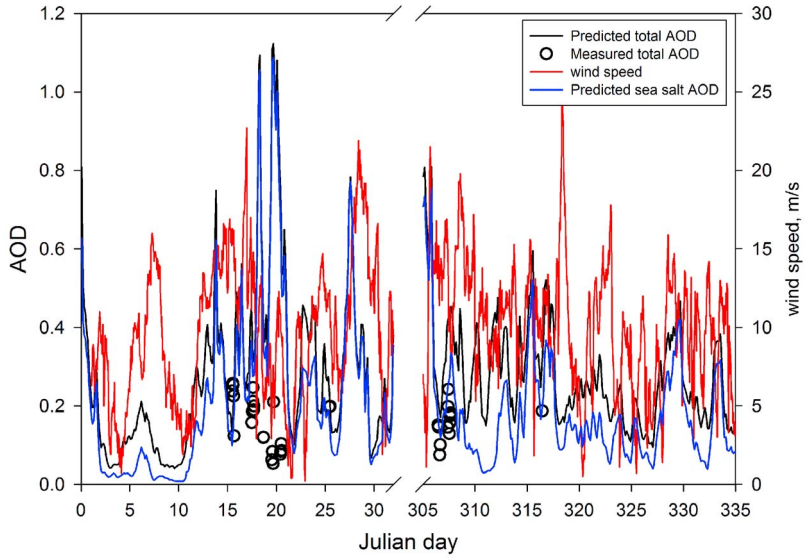

Figure 21. Time series during January and November 2003 at Mace Head for observed wind speed (red line, right *y* axis) and total AOD (black circles, left *y* axis), as well as simulated total (black line) and partial SS AOD (blue line) from the DIRECT simulation; values represent 3 h averages.

during the summer events, the measured sea salt mass concentrations were slightly lower when compared to winter, with 16 and 10 $\mu g/m^3$ for May and June, respectively. Long-term observations of seasonal patterns of aerosol chemical species over the Northeast Atlantic confirm that sea salt mass concentrations are lower during summer, due to the composite effect of lower wind speed and enhanced contribution of biogenic organic compounds [*Yoon et al.*, 2007]. The latter applies to mainly submicron particles due to the thermodynamic substitution effect of sea salt by biogenic organic matter in primary produced sea spray [*O'Dowd et al.*, 2004].

[53] There is a better agreement between simulated total AOD and observations for the summer period when model sea salt is far less dominating model total AOD compared to the winter period. This is partly due to a better agreement between predicted and observed wind speed during summer (median error below 1%) compared to winter (median error of +24%) (D. Ceburnis et al., Validation of aerosol chemical components predicted by the ECMWF IFS model, manuscript in preparation, 2010, hereafter Ceb2010). Apart from sea salt and dust, the IFS model only takes into account anthropogenic sulfate, organic matter and black carbon, and it does not consider biogenic sulfate and organic carbon

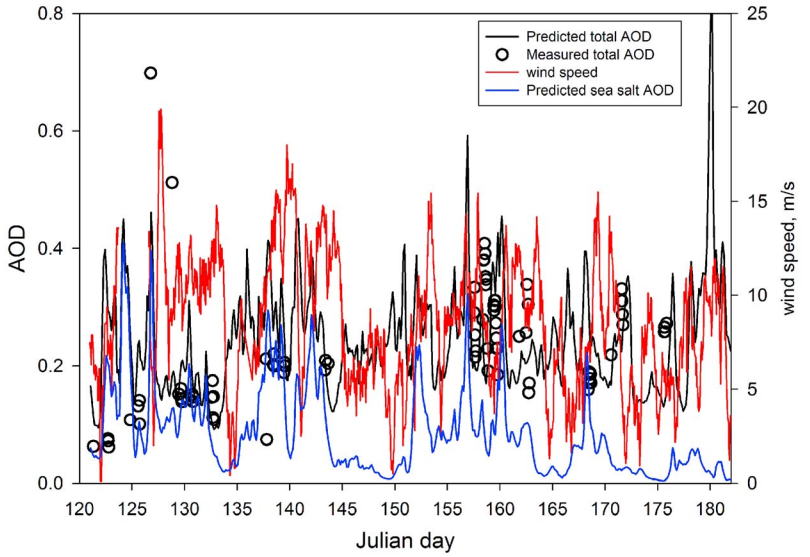

Figure 22. Time series during May and June 2003 at Mace Head for observed wind speed (red line, right *y* axis) and total AOD (black circles, left *y* axis), as well as simulated total (black line) and partial SS AOD (blue line) from the DIRECT simulation; values represent 3 h averages.

emissions. It has become established that biogenic organic matter in sea spray and biogenic sulfate can contribute significantly to aerosol loadings during periods of high biological activity [*O'Dowd et al.*, 2004; *Yoon et al.*, 2007]. MODIS seasonal composite images for that period reveal a complex spatial pattern of AOD values over the North Atlantic, indicative of organic carbon in sea spray yet unaccounted in the IFS model. *Vignati et al.* [2010] presented a modeling case highlighting the global significance of biogenic organic matter. Taking into account biogenic organic matter and sulfate in the IFS model would increase the discrepancy between model and observations. However, it was already mentioned that anthropogenic sulfate is largely overestimated by the model (section 4.1.2), which in a way compensates for the absence of biogenic component, especially over oceanic locations, leading to the reasonable agreement between the aerosol model and observations.

5. Discussion

[54] Although GEMS-Aerosol features a global assimilation and forecast system, this study focuses on results for the European scale because of the relevance of a well characterized modeled aerosol state of the atmosphere as boundary condition for European regional air quality models. The global and regional perspective regarding total and partial AOD, fine- and coarse-mode AOD, surface mass concentration, and seasonality is treated in more detail by SchulzetalPartIV2010.

[55] Model evaluation encompasses several difficulties. Whereas model output is regularly available on a spatial and temporal scale, available observational aerosol optical data is often sparse and incomplete. For example, there are many AERONET stations in Europe, but not in Africa. In addition, AERONET AOD data is available for clear skies only. Further, measurement data often cannot be taken just as is, but care has to be taken of instrumental errors, or environmental biases like, for example, radiometric artifacts or thin to subvisible cirrus clouds affecting Sun photometer measurements. Finally, also model uncertainties related to simulated aerosol types and size bins, the radiative transfer scheme, or the assimilation technique (see companion papers by *Benedetti et al.* [2009] and *Morcrette et al.* [2009]) have to be taken into account when interpreting the results. The high bias of ASSIM with respect to the observations can be associated with the prescribed observation error. As the MODIS product does not come with a pixel-by-pixel error, but rather with a statistical error model derived from comparisons with independent AERONET data, the observation error can be prescribed as a function of the observed AOD value. This implies that in an absolute sense the errors are larger for large values of AOD, which might not be always true.

[56] The quality of the results depends not only on the dynamics of the model and the adequacy of the aerosol physical parameterizations, but also on the representativeness of the sources. As the aerosol model calculates the aerosol optical depth from mass extinction coefficients, the source functions and emissions used are essential. The forecast model is very sensitive to the sources, with a large dependence on the inventories or climatologies used for the anthropogenic aerosols, and on the details of the sea salt and desert dust parameterizations. Outdated emission data are likely to introduce biases. Recent developments in secondary organic aerosol prediction [*Robinson et al.*, 2007; *Lane et al.*, 2008] and primary biogenic organic aerosol prediction [*Vignati et al.*, 2010] may be useful for future aerosol model improvements.

[57] In the case of sea salt, Ceb2010 found that the total sea salt mass concentration is significantly overpredicted by the model at all investigated observation stations. Ceb2010 made a detailed analysis of the simulated and observed wind speed, and the sea salt aerosol sampling setup, revealing that comparing only the model SS PM10 and not total mass with the observations yields much closer agreements. This implies that the majority of particles above 10 μm do not get sampled. However, it cannot be excluded that the sea salt source function is too strong, particularly at higher wind speed. Very low sea salt mass concentrations are generally underestimated, which could be interpreted by either too efficient removal processes or shortcomings of the source function.

[58] With respect to the simulation of the Saharan dust event in March 2004 and the pronounced underestimation of total AOD in the core of the plume compared to SEVIRI total AOD, it should be noted that SEVIRI AOD data show a high bias against MODIS AOD, in particular at low AOD values, where SEVIRI also reveals more noise [*De Paepe et al.*, 2008]. The high bias, however, is more pronounced at the longer wavelength bands 830 and 1610 nm than for 630 nm. In addition, SEVIRI comparisons with MODIS reveal a high correlation (0.96 for MODIS Terra, 0.91 for MODSI Aqua). Furthermore, independent comparisons by different satellite systems (SEVIRI, ATSR (Along Track Scanning Radiometer), MODIS), of the AOD in the core of similar dust plumes coming out of Sahara in March 2006 (part of the GLOBAEROSOL project, see www.globaerosol.info/project_description/publications.htm; user_report), showed that the retrieved AOD varied by up to 30%.

[59] In the case of desert dust aerosol and the model capability to simulate fine- and coarse-mode AOD, it has to be noted that the system assimilates total AOD and cannot influence separately the coarse and fine particles. If the DIRECT simulation underestimates total AOD, the analysis reacts by increasing the mass of both fine- and coarse-mode aerosols, resulting in an overestimation of the coarse mode, as illustrated in Figure 20. The assimilation of fine-mode AOD could help to improve this point. A refinement of the dust source function could be envisaged as well. The inclusion of gustiness [*Engelstaedter and Washington*, 2007] was already tested with improved agreements with surface observations at dust dominated sites [*Morcrette et al.*, 2008] and might be included in a future aerosol model version.

[60] Concerning the comparisons of model total AOD at 550 and 865 nm at Lille, Dunkerque and Toulon with POLDER-2 fine-mode AOD at these wavelengths (Figure 9), it is important to recall that the GEMS aerosol model does not directly simulate fine-mode AOD. Although model fine-mode AOD can be approximated as a sum of the partial BC, OM, and SU AODs, there are no model fine fraction AODs for desert dust and sea salt what could be problematic if desert dust or sea salt was present. On the other side, please note that the purpose of this comparison is to trace the effect

of the assimilation procedure. Further on, the analysis is completed by the comparison of total model AOD against total AERONET AOD in Figure 10.

[61] Furthermore, the representativeness of the individual observation stations and the selection of sites is critical. Given that a model value is representative of a grid cell of the coarse horizontal resolution of the model, a strong local aerosol source at a certain station can distort the comparison when not accounted for. However, it is interesting to note that for the Dunkerque site, which is attributed to a strong local source of industrial and urban pollution, the performance of the model was only slightly improved after assimilation of MODIS AOD. Regarding the PM comparisons of this study, the aerosol concentration at the ground level at the PM measurement site may differ from the concentration at elevated layers in non-well-mixed atmospheres, in addition to the issue of representativeness of the site to the true spatial aerosol distribution. However, the sampling sites, whose data are used for the PM analysis, are located in densely populated and industrial areas that provide the main emission sources of anthropogenic aerosols, and the model and observed AOD agree reasonably well. The aerosol model species and size bins can generally be combined to reconstruct approximate PM2.5 concentrations, which in case of agreement with observations provide confidence that the model contains useful information on the aerosol composition at the surface level.

[62] For the assimilation system it is a demanding test to be compared with surface aerosol species concentrations, since the evaluation is looking into a surface mass concentration, while total aerosol optical depth is used to correct aerosol column loads. Any error in aerosol composition, optical aerosol model and vertical distribution will be amplified. Whereas sea salt and desert dust aerosol predictions are based on physical process parameterization, organic matter, black carbon and sulfate aerosols are predicted based on annual, monthly, or 8 day mean emission data. The discrepancies shown in this study between observed and modeled PM2.5 concentrations can result from an overestimation of the emitted mass, inadequate emission inventories, in the case of SO_4 too efficient and rapid conversion of SO_2 to SO_4 and too weak dry deposition, or discrepancies in the aerosol vertical profile.

[63] Ceb2010 investigated the performance of the GEMS aerosol model with respect to surface mass concentrations. They found that the assimilation of MODIS AOD does not improve significantly the simulation of the mass concentrations of the individual species, however, the correlations between model and observations are mostly statistically significant. More high-quality chemical observations of longer time periods would help to facilitate such an evaluation.

[64] With respect to the aerosol vertical distribution of wild fire aerosol in the model, it is necessary to recall that only total column AOD is assimilated with no information on the vertical distribution of aerosols entering the assimilation system. Although the assimilation can correct in a limited way, the initialization of the emissions at the right heights is essential for the simulation of transport and dispersion. In particular, a higher resolution in both space and time for the emission of fire-related particles would be beneficial. The SEVIRI fire radiative product [*Kaiser et al.*, 2009] fulfills this requirement and its use, together with that of a forest fire injection height, is planned for a future aerosol model version.

6. Summary and Conclusions

[65] This study presents the evaluation of the GEMS aerosol assimilation and forecast system by means of case studies. It complements the work of *Benedetti et al.* [2009], *Morcrette et al.* [2009] and SchulzetalPartIV2010. The GEMS aerosol modeling system is novel as it is the first aerosol model fully coupled to a NWP model with data assimilation. Three specific events were examined: periods of high and low sea salt production, a large Saharan dust event in March 2004, and the summer heat wave in August 2003 in Europe, characterized by forest fire aerosol and conditions of high temperatures and stagnation, favoring photochemistry and secondary aerosol formation.

[66] The aerosol model simulated winter sea salt AOD reasonably well, however, showing a general overestimation. Agreement was better during summer events, when the simulated partial sea salt AOD dominated much less total AOD. Such an agreement suggests that over oceanic regions the natural biogenic sources are masked by overestimated model anthropogenic aerosol species. Sea salt simulation could be improved by refinements in the sea salt source function and wind speed modeling. The inclusion of a contribution by biogenic organic matter in sea spray due to enhanced biological activity in oceanic surface waters, yet unaccounted in the aerosol model, might also have positive effects.

[67] The Saharan dust storm analysis demonstrated that transport and atmospheric dynamics were simulated reasonably well in the model. The horizontal locations of the main features of the aerosol distribution were well captured, as well as the timing of the AOD peaks. At locations close to the dust source regions, the DIRECT simulation underestimated the AOD, especially peaks. This suggests that the model underestimates the emission intensity in the Sahara. The assimilation of MODIS AOD at 550 nm improved significantly model performance, including the AOD peaks, and also AOD predictions for regions without MODIS data for assimilation (bright desert surfaces). Compared to AOD retrieved from SEVIRI, the DIRECT version showed a distinct underestimation. This low bias was reduced, but still present, in the ASSIM version, both at low and high AOD values. The assimilation had little impact on correcting the DIRECT version in terms of the Angström exponent and thus the dust size distribution. The Angström exponent was largely overestimated at Dakar and Capo Verde, but better matched at El Arenosillo, revealing that the fine-mode aerosol is overestimated in the aerosol model.

[68] The aerosol model captured the distinct increase of sulfate mass concentration during the summer heat wave period in 2003 in Europe very well. The linear regression correlation coefficients between modeled and observed sulfate mass concentrations were highly significant in the range of 0.50–0.67. However, the model overestimated significantly the observed sulfate mass concentration.

[69] The Portuguese wild fires of summer 2003 provided the possibility to investigate the aerosol model capability to simulate the spatial transport of the fire plume aerosols. Graphs of POLDER-2 mean fine-mode AOD at 550 nm and

the DIRECT and ASSIM simulation results of the mean fine-mode AOD at 550 nm for 5 to 6 August 2003 showed that the simulations agreed reasonably well with the general pattern of areas of elevated fine-mode aerosol observed by POLDER-2, however, missing some decisive elevated AOD areas and both overestimating and underestimating the observations in other areas. The assimilation did not improve the overall pattern significantly. Within the model, only sulfate contributed significantly to the fine-mode AOD in the aerosol plume. OM played a minor part and BC only a marginal one, although in a smoke plume these species should be stronger represented.

[70] The correlation coefficient for simulated (ASSIM version) against measured PM2.5 was 0.71 for the period end of July until mid-August 2003 and for the three sites Lille, Dunkerque/Calais and Toulon/Marseille. This good correlation is encouraging considering the low spatial resolution of the model and the local character of PM measurements. The correlation coefficient degraded for measured AOD against measured PM2.5 (r = 0.47), and it degraded even stronger for the comparison of modeled AOD against measured PM2.5 (r = 0.40).

[71] With respect to the total AOD predictions during the summer heat wave period, the aerosol model matched well the observed overall AOD level and the day-to-day variability at the investigated sites, although the model missed or underestimated some peaks. With the assimilation the total AOD peaks were better matched, due to increased sulfate AOD, consistent with increased sulfate PM2.5 mass. The correlation coefficients for the sites ranged from 0.70 to 0.86.

[72] The assimilation of MODIS AOD data improved the subsequent aerosol predictions when compared with observations, in particular concerning the correlation and AOD peak values. The assimilation was less effective in correcting a positive (PM2.5, sulfate mass concentration, Angström exponent) or negative (desert dust plume AOD) model bias. The development of a successful aerosol analysis was therefore fundamental to the quality of the subsequent aerosol forecast, and thus also to the provision of boundary conditions for regional air quality models. This study further demonstrated the importance of combining model and observations for an accurate evaluation and monitoring of (anthropogenic) aerosol impacts.

[73] There is obviously room for improvements, in particular more up-to-date emission inventories and a better characterization of the sources of (anthropogenic) aerosols, including primary biogenic organic and secondary organic aerosol prediction. Furthermore, the vertical distribution of the (anthropogenic) aerosols could be improved via a plume model, the assimilation of vertical profiles of the extinction coefficient (using ground-based or spaceborne lidar data), and the introduction of the injection height for smoke aerosols (SEVIRI Fire Radiation Power product). In addition, the inclusion of stratospheric aerosol, a more detailed sulfate chemistry scheme, and an assimilation of fine-mode AOD might prove useful. However, global operational numerical weather prediction models cannot readily implement the chemical complexity of regional models or specific chemical transport models, and thus case studies are challenging for such a global resolution model. GEMS will be continued within the European Commission's FP7 project MACC (Monitoring Atmospheric Composition and Climate, www.gmes-atmosphere.eu).

[74] **Acknowledgments.** The authors would like to thank all members of the GEMS-AER team. We thank EPA Ireland for financial support of D. Ceburnis and for providing observation data. At LOA, Didier Tanré and Fabrice Ducos are thanked for their helpful contribution to the analysis of POLDER and AERONET data for the pollution aerosol case study. We also thank P. Goloub, S. Despiau, D. Tanré, V. E. Cachorro, and D. V. Henriques, who are the principal investigators of the AERONET/PHOTONS and Brewer sites used for this study. We thank ADEME for providing the PM2.5 data. O.B. was supported by the joint DECC and Defra Integrated Climate Programme–DECC/Defra (GA01101). In particular, we are grateful to A. Hollingsworth, who initiated and led the GEMS project. GEMS was funded by the European Commission's Framework Programme 6, contract 516099.

References

Barrie, L., et al. (2004), International Global Atmospheric Chemistry Observations System (IGACO) theme report, *ESA SP-1282*, WMO, Geneva, Switzerland.

Benedetti, A., et al. (2009), Aerosol analysis and forecast in the European Centre for Medium-Range Weather Forecasts Integrated Forecast System: 2. Data assimilation, *J. Geophys. Res.*, *114*, D13205, doi:10.1029/2008JD011115.

Bréon, F.-M., and S. Colzy (1999), Cloud detection from the spaceborne POLDER instrument and validation against surface synoptic observations, *J. Appl. Meteorol.*, *36*, 777–785.

Cheymol, A., L. G. Sotelino, K. S. Lam, J. Kim, A. M. Siani, and H. De Backer (2009), Intercomparison of Aerosol Optical Depth from Brewer ozone spectrophotometers and CIMEL sunphotometer measurements, *Atmos. Chem. Phys.*, *9*, 733–741.

Collins, W. D., P. J. Rasch, B. E. Eaton, B. V. Khattatov, J.-F. Lamarque, and C. S. Zender (2001), Simulating aerosols using a chemical transport model with assimilation of satellite aerosol retrievals: Methodology for INDOEX, *J. Geophys. Res.*, *106*(D7), 7313–7336, doi:10.1029/2000JD900507.

Dentener, F., et al. (2006), Emissions of primary aerosol and precursor gases in the years 2000 and 1750 prescribed data-sets for AeroCom, *Atmos. Chem. Phys.*, *6*, 4321–4344.

De Paepe, B., A. Ignatov, S. Dewitte, and A. Ipe (2008), Aerosol retrieval over ocean from SEVIRI for the use in GERB Earth's radiation budget analyses, *Remote Sens. Environ.*, *112*(5), 2455–2468.

Deuzé, J.-L., et al. (2001), Remote sensing of aerosols over land surfaces from POLDER-ADEOS-1 polarized measurements, *J. Geophys. Res.*, *106*(D5), 4913–4926, doi:10.1029/2000JD900364.

Dubovik, O., A. Smirnov, B. N. Holben, M. D. King, Y. J. Kaufman, T. F. Eck, and I. Slutsker (2000), Accuracy assessments of aerosol optical properties retrieved from Aerosol Robotic Network (AERONET) Sun and sky radiance measurements, *J. Geophys. Res.*, *105*(D8), 9791–9806.

Dubovik, O., B. Holben, T. F. Eck, A. Smirnov, Y. J. Kaufman, M. D. King, D. Tanré, and I. Slutsker (2002), Variability of absorption and optical properties of key aerosol types observed in worldwide locations, *J. Atmos. Sci.*, *59*(3), 590–608.

Engelstaedter, S., and R. Washington (2007), Temporal controls on global dust emissions: The role of surface gustiness, *Geophys. Res. Lett.*, *34*, L15805, doi:10.1029/2007GL029971.

Ginoux, P., M. Chin, I. Tegen, J. Prospero, B. N. Holben, O. Dubovik, and S.-J. Lin (2001), Sources and distributions of dust aerosols simulated with the GOCART model, *J. Geophys. Res.*, *106*(D17), 20,255–20,274, doi:10.1029/2000JD000053.

Hodzic, A., R. Vautard, H. Chepfer, P. Goloub, L. Menut, P. Chazette, J. L. Deuzé, A. Apituley, and P. Couvert (2006), Evolution of aerosol optical thickness over Europe during the August 2003 heat wave as seen from CHIMERE model simulations and POLDER data, *Atmos. Chem. Phys.*, *6*, 1853–1864.

Hodzic, A., S. Madronich, B. Bohn, S. Massie, L. Menut, and C. Wiedinmyer (2007), Wildfire particulate matter in Europe during summer 2003: Mesoscale modeling of smoke emissions transport and radiative effects, *Atmos. Chem. Phys.*, *7*, 4043–4064.

Holben, B. N., et al. (2001), An emerging ground-based aerosol climatology: Aerosol optical depth from AERONET, *J. Geophys. Res.*, *106*(D11), 12,067–12,097, doi:10.1029/2001JD900014.

Hollingsworth, A., et al. (2008), Toward a monitoring and forecasting system for atmospheric composition: The GEMS project, *Bull. Am. Meteorol. Soc.*, *89*(8), 1147–1164.

Huneeus, N., O. Boucher, and F. Chevalier (2009), Simplified aerosol modeling for variational data assimilation, *Geosci. Model Dev.*, *2*, 213–229.

Ignatov, A., and L. Stowe (2002), Aerosol retrievals from individual AVHRR channels. Part 1: Retrieval algorithm and transition from Dave to 6S radiative transfer model, *J. Atmos. Sci.*, *59*(3), 313–334.

Intergovernmental Panel on Climate Change (IPCC) (2007), *Climate Change 2007: The Physical Science Basis. Contribution of Working Group I to the Fourth Assessment Report of the Intergovernmental Panel on Climate Change*, edited by S. Solomon et al., 996 pp., Cambridge University Press, Cambridge, U. K.

Kacenelenbogen, M., J. F. Léon, I. Chiapello, and D. Tanré (2006), Characterization of aerosol pollution events in France using ground-based and POLDER-2 satellite data, *Atmos. Chem. Phys.*, *6*, 4843–4849.

Kaiser, J. W., M. Suttie, J. Flemming, J.-J. Morcrette, O. Boucher, and M. G. Schultz (2009), Global real-time fire emission estimates based on space-borne fire radiative power observations, *AIP Conf. Proc.*, *1100*, 645–648.

Knippertz, P., and A. H. Fink (2007), Synoptic and dynamic aspects of an extreme springtime Saharan dust outbreak, *Q. J. R. Meteorol. Soc.*, *132*(617), 1153–1177.

Lane, T. E., N. M. Donahue, and S. N. Pandis (2008), Simulating secondary organic aerosol formation using the volatility basis-set approach in a chemical transport model, *Atmos. Environ.*, *42*(32), 7439–7451.

Levy, R. C., L. A. Remer, S. Mattoo, E. F. Vermote, and Y. J. Kaufman (2007), Second-generation operational algorithm: Retrieval of aerosol properties over land from inversion of Moderate Resolution Imaging Spectrometer spectral reflectance, *J. Geophys. Res.*, *112*, D13211, doi:10.1029/2006JD007811.

Monahan, E. C., K. L. Davidson, and D. E. Spiel (1982), Whitecap aerosol productivity deduced from simulation tank measurements, *J. Geophys. Res.*, *87*(C11), 8898–8904, doi:10.1029/JC087iC11p08898.

Morcrette, J.-J., A. Beljaars, A. Benedetti, L. Jones, and O. Boucher (2008), Sea-salt and dust aerosol in the ECMWF IFS model, *Geophys. Res. Lett.*, *35*, L24813, doi:10.1029/2008GL036041.

Morcrette, J.-J., et al. (2009), Aerosol analysis and forecast in the European Centre for Medium-Range Weather Forecasts Integrated Forecast System: Forward modeling, *J. Geophys. Res.*, *114*, D06206, doi:10.1029/2008JD011235.

Mulcahy, J., C. D. O'Dowd, S. G. Jennings, and D. Ceburnis (2008), Significant enhancement of aerosol optical depth in marine air under high wind conditions, *Geophys. Res. Lett.*, *35*, L16810, doi:10.1029/2008GL034303.

Mulcahy, J., C. D. O'Dowd, and S. G. Jennings (2009), Aerosol optical depth in clean marine and continental northeast Atlantic air, *J. Geophys. Res.*, *114*, D20204, doi:10.1029/2009JD011992.

O'Dowd, C. D., and M. H. Smith (1993), Physico-chemical properties of aerosol over the northeast Atlantic: Evidence for wind speed related submicron sea-salt aerosol production, *J. Geophys. Res.*, *98*(D1), 1137–1149, doi:10.1029/92JD02302.

O'Dowd, C. D., M. C. Facchini, F. Cavalli, D. Ceburnis, M. Mircea, S. Decesari, S. Fuzzi, Y. J. Yoon, and J.-P. Putaud (2004), Biogenically driven organic contribution to marine aerosols, *Nature*, *431*, 676–680.

Reddy, M. S., O. Boucher, N. Bellouin, M. Schulz, Y. Balkanski, J.-L. Dufresne, and M. Phan (2005), Estimates of global multicomponent aerosol optical depth and direct radiative perturbation in the Laboratoire de Météorologie Dynamique General Circulation Model, *J. Geophys. Res.*, *110*, D10S16, doi:10.1029/2004JD004757.

Remer, L. A., et al. (2005), The MODIS aerosol algorithm, products and validation, *J. Atmos. Sci.*, *62*(4), 947–973.

Robinson, A. L., N. M. Donahue, M. K. Shrivastava, E. A. Weitkamp, A. M. Sage, A. P. Grieshop, T. E. Lane, J. R. Pierce, and S. N. Pandis (2007), Rethinking organic aerosols: Semivolatile emissions and photochemical aging, *Science*, *315*(5816), 1259–1262.

Schulz, M., G. De Leeuw, and Y. Balkanski (2004), Sea-salt aerosol source functions and emissions, in *Emission of Atmospheric Trace Compounds*, edited by C. Granier, P. Artaxo, and C. E. Reeves, pp. 333–359, Kluwer Acad., Norwell, Mass.

Smith, M. H., and N. M. Harrison (1998), The sea spray generation function, *J. Aerosol Sci.*, *29*, Suppl. 1, S189–S190.

Tegen, I., P. Hoorig, M. Chin, I. Fung, D. Jacob, and J. Penner (1997), Contribution of different aerosol species to the global aerosol extinction optical thickness: Estimates from model results, *J. Geophys. Res.*, *102*(D20), 23,895–23,915, doi:10.1029/97JD01864.

Tressol, M., et al. (2008), Air pollution during the 2003 European heat wave as seen by MOZAIC airliners, *Atmos. Chem. Phys.*, *8*, 2133–2150.

van der Werf, G. R., J. T. Randerson, L. Giglio, G. J. Collatz, P. S. Kasibhatla, and A. F. Arellano Jr. (2006), Interannual variability in global biomass burning emissions from 1997 to 2004, *Atmos. Chem. Phys.*, *6*, 3423–3441.

Vautard, R., et al. (2007), Evaluation and intercomparison of ozone and PM10 simulations by several chemistry transport models over four European cities within the CityDelta project, *Atmos. Environ.*, *41*(1), 173–188.

Vignati, E., M. C. Facchini, M. Rinaldi, C. Scannell, D. Ceburnis, J. Sciare, M. Kanakidou, S. Myriokefalitakis, F. Dentener, and C. D. O'Dowd (2010), Global scale emission and distribution of sea spray aerosol: Sea-salt and organic enrichment, *Atmos. Environ.*, *44*(5), 670–677.

Weaver, C., A. da Silva, M. Chin, P. Ginoux, O. Dubovik, D. Flittner, A. Zia, L. Remer, B. Holben, and W. Gregg (2007), Direct insertion of MODIS radiances in a global aerosol transport model, *J. Atmos. Sci.*, *64*, 808–826, doi:10.1175/JAS3838.1.

Wehrli, C. (2004), GAWPFR: A network of aerosol optical depth observations with precision filter radiometers, in *WMO/GAW Experts Workshop on a Global Surface-Based Network for Long Term Observations of Column Aerosol Optical Properties*, edited by U. Baltensperger, L. Barrie, and C. Wehrli, *WMO TD 1287*, pp. 36–38, WMO, Geneva, Switzerland.

Yoon, Y. J., D. Ceburnis, C. D. O'Dowd, S. G. Jennings, O. Jourdan, F. Cavalli, M. C. Facchini, S. Decesari, L. Emblico, and S. Fuzzi (2007), Seasonal characteristics of the physicochemical properties of marine atmospheric aerosols over the North Atlantic, *J. Geophys. Res.*, *112*, D04206, doi:10.1029/2005JD007044.

Yttri, K. E., et al. (2007), Elemental and organic carbon in PM10: A one year measurement campaign within the European Monitoring and Evaluation Programme EMEP, *Atmos. Chem. Phys.*, *7*, 5711–5725.

Yu, H., R. E. Dickinson, M. Chin, Y. J. Kaufman, M. Zhou, L. Zhou, Y. Tian, O. Dubovik, and B. N. Holben (2004), Direct radiative effect of aerosols as determined from a combination of MODIS retrievals and GOCART simulations, *J. Geophys. Res.*, *109*, D03206, doi:10.1029/2003JD003914.

Zhang, J., J. S. Reid, D. L. Westphal, N. L. Baker, and E. J. Hyer (2008), A system for operational aerosol optical depth data assimilation over global oceans, *J. Geophys. Res.*, *113*, D10208, doi:10.1029/2007JD009065.

A. Benedetti and J.-J. Morcrette, European Centre for Medium-range Weather Forecasts, Shinfield Park, Reading RG2 9AX, UK.

O. Boucher, Met Office Hadley Centre, FitzRoy Road, Exeter EX1 3PB, UK.

D. Ceburnis and C. D. O'Dowd, School of Physics and Centre for Climate and Air Pollution Studies, Environmental Change Institute, National University of Ireland Galway, University Road, Galway, Ireland.

I. Chiapello, Y. Derimian, and J.-F. Léon, Laboratoire d'Optique Atmosphérique, CNRS/Université de Lille 1, Bat. P5, F-59655 Villeneuve d'Ascq CEDEX, France.

H. De Backer, B. De Paepe, S. Dewitte, and A. Mangold, Observations Department, Royal Meteorological Institute of Belgium, Av. Circulaire 3, B-1180 Brussels, Belgium. (alexander.mangold@oma.be)

H. Flentje, Meteorologisches Observatorium Hohenpeissenberg, Deutscher Wetterdienst, Albin-Schwaiger-Weg 10, D-82383 Hohenpeissenberg, Germany.

N. Huneeus and M. Schulz, Laboratoire des Sciences du Climat et de l'Environnement, CEA/CNRS/UVSQ, L'Orme des Merisiers, Bat. 712, Point Courrier 132, F-91191 Gif-sur-Yvette, France.

M. Kacenelenbogen, ORAU/NASA Ames Research Center, MS 245-5, Bldg. 245, PO Box 1, Moffett Field, CA 94035-0001, USA.

S. Kinne, Max-Planck Institute for Meteorology, Bundesstr. 53, D-20146 Hamburg, Germany.